


ARTICLE

Slc7a5 alters Kv β -mediated regulation of Kv1.2

Shawn M. Lamothe and Harley T. Kurata 

The voltage-gated potassium channel Kv1.2 plays a pivotal role in neuronal excitability and is regulated by a variety of known and unknown extrinsic factors. The canonical accessory subunit of Kv1.2, Kv β , promotes N-type inactivation and cell surface expression of the channel. We recently reported that a neutral amino acid transporter, Slc7a5, alters the function and expression of Kv1.2. In the current study, we investigated the effects of Slc7a5 on Kv1.2 in the presence of Kv β 1.2 subunits. We observed that Slc7a5-induced suppression of Kv1.2 current and protein expression was attenuated with cotransfection of Kv β 1.2. However, gating effects mediated by Slc7a5, including disinhibition and a hyperpolarizing shift in channel activation, were observed together with Kv β -mediated inactivation, indicating convergent regulation of Kv1.2 by both regulatory proteins. Slc7a5 influenced several properties of Kv β -induced inactivation of Kv1.2, including accelerated inactivation, a hyperpolarizing shift and greater extent of steady-state inactivation, and delayed recovery from inactivation. These modified inactivation properties were also apparent in altered deactivation of the Kv1.2/Kv β /Slc7a5 channel complex. Taken together, these findings illustrate a functional interaction arising from simultaneous regulation of Kv1.2 by Kv β and Slc7a5, leading to powerful effects on Kv1.2 expression, gating, and overall channel function.

Introduction

Kv1.2 has been a valuable model to study the function and regulation of ion channels, as it was the first eukaryotic voltage-gated potassium channel with a reported atomic resolution structure (Long et al., 2005). Kv1.2 plays an essential role in the nervous system, where it regulates membrane excitability and action potential propagation (Bean, 2007; Bekkers and Delaney, 2001; Guan et al., 2007). In dorsal root ganglion neurons, Kv1.2 is involved in nociception and generation of neuropathic pain (Ishikawa et al., 1999; Yang et al., 2004). In the brain, Kv1.2 dysfunction results in a spectrum of seizure disorders and neurodevelopmental delay (Pena and Coimbra, 2015; Allen et al., 2016; Syrbe et al., 2015; Sachdev et al., 2017; Masnada et al., 2017; Corbett et al., 2016). While recent identification of genetic mutations in KCNA2 (Kv1.2) with next-generation sequencing have assisted in the understanding of a genotype/phenotype correlation for epilepsy, interpretation of these findings requires further consideration since our understanding of ion channel regulation and modification by extrinsic factors is likely incomplete.

Although there is a detailed understanding of intrinsic mechanisms of voltage-dependent gating of Kv1.2, these channels also associate with a variety of extrinsic regulators that alter channel behavior. Tyrosine-dependent phosphorylation of Kv1.2 by tyrosine kinase, RhoA, suppresses channel function and expression (Cachero et al., 1998; Stirling et al., 2009).

Phosphorylation accelerates endocytosis of the channel through enhanced interaction with the cytoskeletal anchoring protein, cortactin (Nesti et al., 2004; Williams et al., 2007). Additionally, cocaine-induced activation of the σ -1 receptor (an ER chaperone protein) influences Kv1.2 by facilitating trafficking of the channel to the cell membrane (Kourrich et al., 2013). Kv1.2 is also sensitive to lipids, as both phosphatidyl inositol bis(4,5)phosphate and phosphatidic acid have been demonstrated to cause a hyperpolarizing shift in channel activation (Kruse and Hille, 2013; Rodriguez-Menchaca et al., 2012; Hite et al., 2014). Nonetheless, the most recognized accessory proteins of Kv1.2, and other Kv1 subtypes, are the Kv β auxiliary subunits. Kv β subunits are cytosolic proteins that assemble in a 1:1 stoichiometry with Kv1 α subunits at the cytoplasmic T1 domain (Gulbis et al., 1999, 2000; Kobertz et al., 2000; Long et al., 2005). There are three mammalian Kv β genes that encode Kv β proteins with alternative splice variants (Kv β 1.1-1.3, Kv β 2.1-2.2, and Kv β 3.1-3.2; Pongs et al., 1999; Pongs and Schwarz, 2010). Assembly of Kv1.2 α -subunits with Kv β isoforms influences subcellular targeting and increases Kv1.2 protein expression, maturation, and cell surface stability (Shi et al., 1996; Heinemann et al., 1995; Gu et al., 2003; Li et al., 2000). Kv1.2 association with Kv β 1 or Kv β 3 confers N-type inactivation of the channel, while Kv β 2 lacks residues in the N-terminus required for the “ball-and-chain” inactivation mechanism (Rettig et al., 1994). Although there is

Department of Pharmacology, Alberta Diabetes Institute, University of Alberta, Edmonton, Alberta, Canada.

Correspondence to Harley Kurata: kurata@ualberta.ca.

© 2020 Lamothe and Kurata. This article is distributed under the terms of an Attribution–Noncommercial–Share Alike–No Mirror Sites license for the first six months after the publication date (see <http://www.rupress.org/terms/>). After six months it is available under a Creative Commons License (Attribution–Noncommercial–Share Alike 4.0 International license, as described at <https://creativecommons.org/licenses/by-nc-sa/4.0/>).

some strain dependence, certain mouse knockout models of Kv β display neurological symptoms, including compromised learning capacity, motor dysfunction, and seizures, along with decreased life expectancy (Giese et al., 1998; McCormack et al., 2002; Connor et al., 2005). Conditions that directly affect Kv β have been shown to impact the frequency of action potential firing in circadian neurons involved with sleep cycles (Kempf et al., 2019; Fogle et al., 2015). Therefore, factors that alter Kv β -mediated regulation of Kv1 channel function can influence a variety of important neurological processes.

We recently reported that a neutral amino acid transporter, Slc7a5, strongly influences function and expression of Kv1.2, possibly mediated by a direct interaction (Baronas et al., 2018). Slc7a5 significantly reduced Kv1.2 total protein and current density and caused a dramatic hyperpolarizing shift in channel activation. Coexpression with Kv β 1.2 did not prevent the Slc7a5-mediated gating shift but rather produced a rapidly inactivating current together with a large hyperpolarizing shift (–50 mV) of channel activation (Baronas et al., 2018). While this demonstrates that Slc7a5 and Kv β subunits can simultaneously coassemble with Kv1.2 channels, the functional outcomes of coexpression of Kv1.2/Slc7a5/Kv β were not studied in detail.

In this study, we explore the functional interaction between Kv1.2, Kv β 1.2 (referred to as Kv β throughout the text), and Slc7a5. Using Western blot and electrophysiological analysis, we observe that coexpression of Kv β with Kv1.2 counteracts the Slc7a5-mediated suppression of Kv1.2 current and protein expression, but not its effects on gating. Concomitant expression of all three proteins generated currents with hallmark features of both Slc7a5 and Kv β modulation, including rapid inactivation and a markedly shifted voltage dependence of activation. The degree of inactivation is greater in the presence of Slc7a5, suggesting that the N-terminal inactivation particle of Kv β binds more favorably to the pore of Kv1.2 when Slc7a5 is present. Consequently, recovery of the channel from inactivation is significantly delayed. Our findings demonstrate that Slc7a5 and Kv β simultaneously assemble with Kv1.2 to dramatically alter channel expression and function. The work expands our knowledge of regulatory complexes of Kv1.2, ultimately contributing to the understanding of neuronal excitability in health and disease.

Materials and methods

Constructs and expression

Kv1.2, Kv1.2[T252R], Kv1.2[L298F], Kv β 1.2 (referred to throughout as Kv β), Kv β 1.2 N-terminal deletion (referred to throughout as Kv β Δ N), Slc7a5, and GFP cDNAs were expressed using the pcDNA3.1(–) vector (Invitrogen), mEGFP-C1, a gift from Michael Davidson (Florida State University, Tallahassee, FL; Addgene plasmid 54759) or mCherry. Where indicated, fluorescent proteins were fused to proteins using standard PCR and compatible restriction digestion and ligation. Constructs were verified by diagnostic restriction digestions and Sanger sequencing (Genewiz or University of Alberta Applied Genomics Core).

Mouse LM(TK–) fibroblast cells (ATCC CCL-1.3, referred to as LM cells throughout) were used for patch-clamp experiments,

whereas HEK293 cells were used for Western blot analysis and coimmunoprecipitation (co-IP) assays because of much higher transfection efficiency. LM and HEK293 cells were cultured and maintained in biolite 25-cm² flasks (Thermo Fisher Scientific) in a 5% CO₂ incubator at 37°C in Dulbecco's modified Eagle medium (DMEM) high glucose (D5671; Sigma-Aldrich) supplemented with 10% FBS and 1% penicillin/streptomycin. Cells were passaged into 12-well plates or 30-mm dishes for Western blot or co-IP, respectively. 24 h later, cells were transfected with cDNAs using jetPRIME transfection reagent (Polyplus). Cotransfection with fluorescent protein cDNA was performed to identify cells for electrophysiological recording by epifluorescence. 6–12 h after transfection, cells were split onto sterile glass coverslips for patch-clamp recordings. Patch-clamp recordings were conducted 24–48 h after transfection. Western blot analysis and co-IP assays were performed 72 h after transfection.

Site-directed mutagenesis

Kv1.2 mutants (Kv1.2[T252R] and Kv1.2[L298F]) were generated by overlap extension PCR as described previously (Ho et al., 1989; Baronas et al., 2018; Rezazadeh et al., 2007). The Kv β 1.2 Δ N mutant was generated by PCR amplification of residues Met77 to Ser 459, using the following primers: forward, 5'-GGGGAATTCATGGCA TACAGGAATCTTGG-3'; reverse, 5'-GGGGAAGCTTTTATGATCTA TAGTCCTTCTTGC-3'. All constructs were expressed using the pcDNA3.1(–) vector (Invitrogen) and verified by diagnostic restriction enzyme digestions and Sanger sequencing (Genewiz or University of Alberta Applied Genomics Core).

Electrophysiology

Patch pipettes were manufactured from soda lime capillary glass (Thermo Fisher Scientific) using a Sutter P-97 (Sutter Instrument) puller. When filled with standard recording solutions, pipettes had a tip resistance of 1–3 M Ω . Recordings were filtered at 5 kHz and sampled at 10 kHz, with manual capacitance compensation and series resistance compensation at 80%, and stored directly on a computer hard drive using an Axopatch 200B amplifier, Digidata 1440 digitizer, and Clampex 10 software (Molecular Devices). Zero current levels are denoted by dashed lines in representative current panels. The external (bath) solution had the following composition (in mM): 135 NaCl, 5 KCl, 1 CaCl₂, 1 MgCl₂, and 10 HEPES, adjusted to pH 7.3 with NaOH. The internal (pipette) solution had the following composition (in mM): 135 KCl, 5 EGTA, and 10 HEPES, adjusted to pH 7.2 using KOH. Chemicals were purchased from Sigma-Aldrich or Thermo Fisher Scientific. Patch-clamp experiments were conducted at room temperature (22 \pm 1°C).

Electrophysiology data analysis

Throughout the text, we have displayed data for all individual cells collected, in addition to reporting descriptive statistics or box plots. Data displayed as line and scatter plots or bar graphs are expressed as mean \pm SD or SEM, as indicated in the figure legends. Box plots depict the median, 25th, and 75th percentiles (box) and the 10th and 90th percentiles (whiskers). Statistical tests used throughout are indicated in the corresponding figure

legends. Conductance–voltage (G–V) relationships were fitted with a Boltzmann equation,

$$G = \frac{1}{[1 + e^{-(V-V_{1/2})/k}]}$$

where *G* is the normalized conductance, *V* is the voltage applied, *V*_{1/2} is the voltage at half-activation, and *k* is a fitted value reflecting the steepness of the curve, in units of mV. G–V relationships were fitted for each individual cell using a least-squares minimization approach in Microsoft Excel (Solver tool). The extracted fit parameters were used for statistical calculations. Current kinetics were fitted with either single or double exponential equations using Clampfit 10.7.

Western blot

Cell lysates from transfected HEK293 cells were collected in NP-40 lysis buffer (1% NP-40, 150 mM NaCl, and 50 mM Tris-HCl) supplemented with 1% protease inhibitor, 72 h after transfection. Proteins were separated using SDS-PAGE gels and transferred onto nitrocellulose membranes. Kv1.2 was detected using a mouse monoclonal Kv1.2 antibody (1:2,000 dilution, clone K14/16 75-008; NeuroMab) and HRP-conjugated goat anti-mouse antibody (1:20,000 dilution, HSO23; Applied Biological Materials). β-Actin was detected using a mouse monoclonal actin antibody (1:1,000 dilution, G043; Applied Biological Materials) and HRP-conjugated goat anti-mouse antibody (1:20,000 dilution, HSO23; Applied Biological Materials). Slc7a5 was detected using a rabbit polyclonal (LAT-1) antibody (1:1,000 dilution, KE026; Transgenic) and HRP-conjugated goat anti-rabbit antibody (1:20,000 dilution, ab6721; Abcam). Kvβ1.2 was detected using a mouse monoclonal antibody (1:500 dilution, clone K47/42; Neuromab). Chemiluminescence was detected using Super-Signal West Femto Max Sensitivity Substrate (Thermo Fisher Scientific) and a FluorChem SP gel imager (Alpha Innotech).

Co-IP

Cell lysates from transfected HEK293 cells were collected in radioimmunoprecipitation assay (RIPA) lysis buffer (1% Triton X-100, 0.5% sodium deoxycholate, 0.1% SDS, 150 mM NaCl, and 50 mM Tris HCl, adjusted to pH 8.0) supplemented with 1% protease inhibitor, 72 h after transfection. 0.5 mg of whole-cell protein lysate in 0.25 ml of RIPA lysis buffer was incubated with appropriate antibodies overnight at 4°C. Kvβ1.2 was precipitated with a mouse anti-Kvβ1.2 primary antibody (clone K47/42; Neuromab). GAPDH was precipitated with a rabbit anti-GAPDH primary antibody (ab9485; Abcam) as a negative control. Protein A/G Plus-agarose beads (sc-2003; Santa Cruz) were added to the protein complexes for 2 h at 4°C. The beads were washed four times with cold RIPA lysis buffer, then resuspended in 2× loading buffer. The samples were boiled for 5 min, and then centrifuged at 10,000 *g* for 5 min. Proteins were separated using 8% SDS-PAGE gels and subjected to Western blot analysis. Kv1.2 was immunoblotted using a mouse monoclonal Kv1.2 antibody (1:2,000 dilution, clone K14/16 75-008; NeuroMab) and HRP-conjugated goat anti-mouse antibody (1:20,000 dilution, HSO23; Applied Biological Materials).

Online supplemental material

The supplemental figures show multiple pieces of raw data (Western blots) or include additional data for experiments that used both WT Kv1.2 and Kv1.2[T252R] channels. Fig. S1 reports the expression of Slc7a5 after coexpression with combinations of Kv1.2 and Kvβ. Fig. S2 presents multiple raw Western blot data illustrating efficient co-IP of Kv1.2 and Kvβ when coexpressed with Slc7a5. Fig. S3 reports the voltage dependence of activation of WT Kv1.2 when coexpressed with various combinations of Slc7a5 and Kvβ, similar to the experiments using Kv1.2[T252R] channels in Fig. 4. Fig. S4 illustrates the effects of Slc7a5 coexpression on Kvβ-mediated inactivation in WT Kv1.2 channels, recapitulating findings for Kv1.2[T252R] shown in Fig. 6. Fig. S5 is a supplement to Fig. 8, and illustrates the kinetics of deactivation of WT Kv1.2 coexpressed with combinations of Slc7a5 and Kvβ, following a depolarizing prepulse to +20 mV. Fig. S6 illustrates the kinetics of Kvβ-mediated inactivation of Kv1.2 with different transfection ratios of Kv1.2 and Kvβ.

Results

Kvβ counteracts Slc7a5-mediated suppression of Kv1.2 current and protein expression

We previously reported that coexpression with Slc7a5 suppresses Kv1.2 currents and protein expression in various cell lines, accompanied by a combination of pronounced gating effects (Baronas et al., 2018). Given the well-established effects of Kvβ subunits on gating and Kv1.2 cell surface maturation and expression (Shi et al., 1996; Heinemann et al., 1995; Li et al., 2000), we sought to determine the regulatory effects of Kvβ and Slc7a5 on Kv1.2. We first established that coexpression of Kv1.2 with Kvβ1.2 (Kvβ) in LM mouse fibroblast cells (1:4 transfection ratio) led to coassembly, which we confirmed by observing a rapidly inactivating current upon depolarization to +60 mV (Fig. 1 A). Deletion of the N-terminal ball-and-chain peptide of Kvβ1.2 (KvβΔN) abolished rapid N-type inactivation of Kv1.2 (Fig. 1 A). Coexpression of Kv1.2 with Kvβ resulted in an increase in current density that was more apparent using KvβΔN (Fig. 1, A and B), indicating that rapid N-type inactivation partially obscured our measurement of peak current density. Coexpression of Kv1.2 with Slc7a5 (1:0.5 transfection ratio) significantly decreased current density (Fig. 1, A and B). However, the inclusion of Kvβ or KvβΔN (1:4:0.5 transfection ratio of Kv1.2:Kvβ:Slc7a5) attenuated Slc7a5-mediated current reduction of the channel with rescue to near-WT levels (Fig. 1 B).

We also tested the effects of Slc7a5 and Kvβ on Kv1.2 protein expression levels in transiently transfected HEK293 cells (Fig. 1, C and D). Kv1.2 generates two prominent bands: a mature fully glycosylated form with a molecular mass of ~80 kD, and an immature core glycosylated band with a molecular mass of ~62 kD (Fig. 1 C). We observed a significant increase in expression of the mature band but not immature Kv1.2 upon coexpression with Kvβ, indicating increased maturation and cell surface stability, consistent with previous reports (Shi et al., 1996; Heinemann et al., 1995; Li et al., 2000). Kv1.2 protein expression was significantly decreased with Slc7a5, for both the mature and immature forms. However, similar to current density

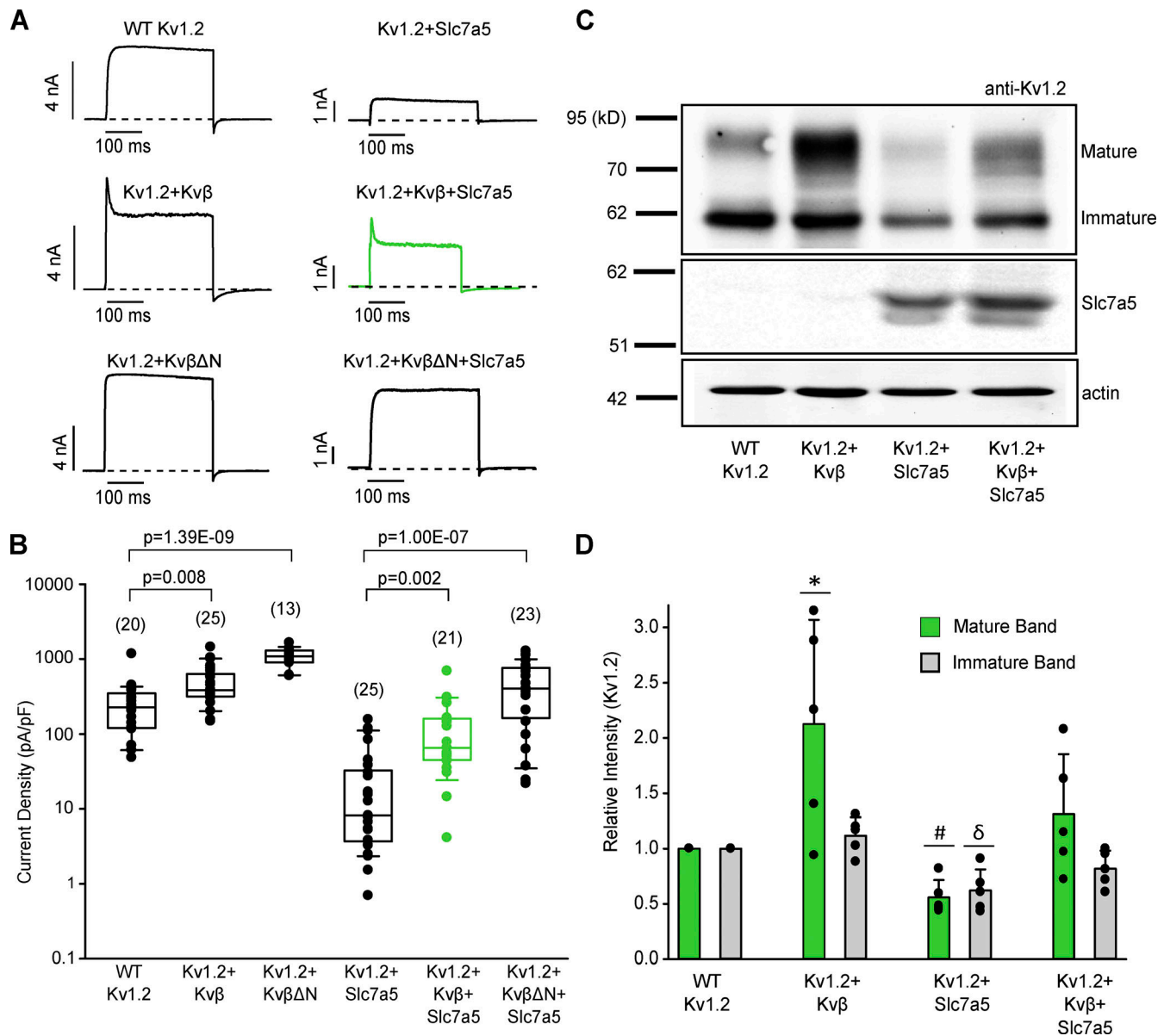


Figure 1. Kvβ offsets Slc7a5-mediated suppression of Kv1.2. (A) Combinations of Kv1.2, mCherry-Slc7a5, Kvβ, KvβΔN, and GFP were expressed in LM cells. Transfection ratios were (with Kv1.2 maintained constant using GFP) Kv1.2:Kvβ or KvβΔN (1:4); Kv1.2:Slc7a5 (1:0.5); and Kv1.2:Kvβ or KvβΔN:Slc7a5 (1:4:0.5). Representative current traces illustrating Kvβ-induced inactivation of Kv1.2 with or without Slc7a5 (300-ms step from -80 mV to +60 mV). (B) Current density was measured as the peak current at +60 mV (from a holding potential of -80 mV). The numbers above the box plots indicate the number of cells examined. A nonparametric Kruskal-Wallis ANOVA on ranks test, followed by a pairwise multiple comparison (Dunn's) post hoc test, was used to compare between groups (P values are denoted above the box plots). (C) Representative Western blot of overexpressed Kv1.2 and Slc7a5 protein from HEK293 cells transfected as in A for 72 h. Actin was used as a loading control. (D) Densitometry measurements of mature (green bars) and immature (gray bars) Kv1.2 protein bands. ANOVA followed by Dunnett's post hoc test was used to compare between groups for each band. Data from individual experiments are superimposed on bars that depict the mean values \pm SD ($n = 5$ independent Western blot experiments). *, $P = 0.016$ relative to the respective WT Kv1.2 mature band; #, $P = 6.67 \times 10^{-5}$ relative to the respective WT Kv1.2 mature band; δ , $P = 0.0008$ relative to the respective WT Kv1.2 immature band. Box plots depict the median, 25th, and 75th percentiles (box) and the 10th and 90th percentiles (whiskers).

measurements, the effect of Slc7a5 was attenuated upon coexpression of Kvβ (Fig. 1, C and D). Coexpression of Slc7a5 with Kv1.2 and Kvβ, separately, did not affect Slc7a5 protein density (Fig. S1). Coexpression of Slc7a5 with Kv1.2 and Kvβ together did not suppress Slc7a5 levels (Fig. 1C, middle panel), indicating that Kvβ-mediated rescue of Kv1.2 from Slc7a5 suppression was not caused by a decrease in Slc7a5 expression.

Kvβ-mediated rescue of Kv1.2 from Slc7a5 suppression may arise from a competitive effect, weakening the interaction with Slc7a5. To address this, we performed a co-IP (Kvβ antibody) of whole-cell proteins extracted from HEK293 cells coexpressing Kv1.2 and Kvβ, with and without Slc7a5. These data illustrate that Slc7a5 does not prevent the association of Kv1.2 and Kvβ (Fig. 2). In many instances, the co-IP of Kv1.2 with the anti-Kvβ

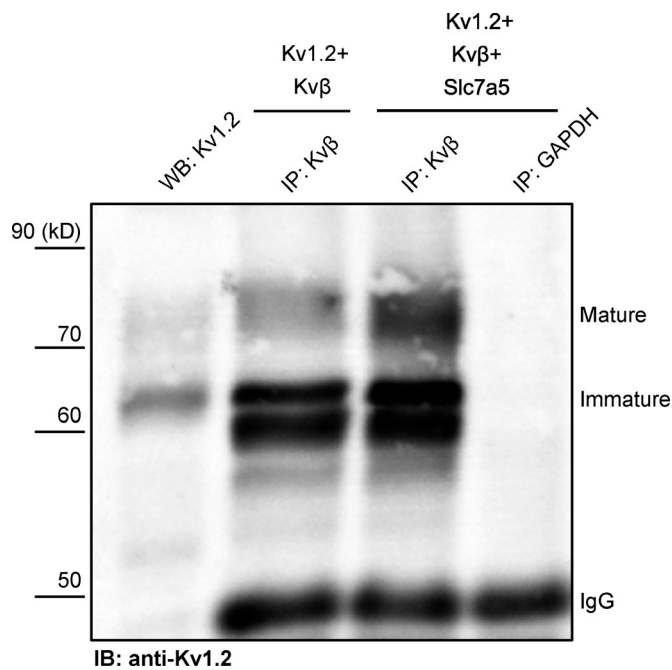


Figure 2. Slc7a5 promotes an interaction between Kv1.2 and Kvβ. Combinations (as indicated in Fig. 1A) of Kv1.2, Slc7a5, Kvβ, and GFP were expressed in HEK293 cells. Co-IP showing that the interaction between Kv1.2 and Kvβ is enhanced in the presence of Slc7a5. GAPDH was used as a negative control. IgG is used as the loading control. WB, Western blotting; IB, immunoblotting. Consistent results were obtained from four independent co-IP experiments (Fig. S2).

antibody appeared stronger when Slc7a5 was coexpressed (Fig. 2 and Fig. S2), especially when considering that overall expression of Kv1.2 is reduced in the presence of Slc7a5. These co-IP findings indicate that the counteracting effects of Slc7a5 and Kvβ on Kv1.2 expression do not arise from competition for interaction with Kv1.2.

A previously described hallmark effect of Slc7a5 is to trap Kv1.2 in a nonconducting state. Although the underlying mechanism is not yet known, this current suppression can be relieved with strong hyperpolarizing holding voltages (−120 mV or more negative), leading to prominent disinhibition of Kv1.2 when it is coexpressed with Slc7a5. We measured disinhibition by recording currents (+10 mV) at 2-s intervals during a 30-s pulse train from a −120-mV holding potential (Fig. 3A). The hyperpolarizing pulse train has little effect when Kv1.2 is expressed alone but causes pronounced enhancement/disinhibition of Kv1.2 coexpressed with Slc7a5 (Fig. 3A). We measured this effect with various combinations of Kv1.2, Kvβ or KvβΔN, and Slc7a5, in Fig. 3B, which illustrates currents before and after the −120-mV pulse train, on a cell-by-cell basis. The disinhibition effect is prominent when Kv1.2 is expressed with Slc7a5, whether or not Kvβ is present (Fig. 3, A and B). We noted a statistical difference in the fold change of Kv1.2 disinhibition (measured as the ratio of the peak current of the first and last +10-mV pulses of the pulse train), with and without Kvβ (Fig. 3C). However, this difference is abolished when a more negative holding voltage is used. That is, prominent further disinhibition was observed for Kv1.2 + Kvβ + Slc7a5 with a holding voltage of

−160 mV, but not for Kv1.2 + Slc7a5 alone (Fig. 3, D and E). This finding suggested that the voltage dependence of the disinhibition effect is shifted by coassembly with Kvβ. Interestingly, this effect is not observed for KvβΔN (Fig. 3, D and E), suggesting that interaction with the N-type inactivation peptide is involved in the altered voltage dependence of disinhibition. These data illustrate that Slc7a5 modulation persists in the presence of Kvβ, and the N-terminal ball-and-chain peptide further stabilizes the channel in an Slc7a5-mediated nonconducting state.

Coregulation of Kv1.2 gating by Slc7a5 and Kvβ

We measured the consequences of coexpression of Slc7a5 and Kvβ on Kv1.2 gating in more detail. Kv1.2 has been reported to exhibit highly variable activation kinetics, with $V_{1/2}$ values ranging from approximately −40 mV to +35 mV in standard conditions (Steidl and Yool, 1999; Grissmer et al., 1994; Rezazadeh et al., 2007; Baronas et al., 2015, 2017). The variability in Kv1.2 activation arises from a unique characteristic of Kv1.2 referred to as use dependence, proposed to be governed by an unidentified extrinsic regulator. Substitution of a threonine to an arginine at amino acid position 252 [T252R], which lies in the cytoplasmic S2–S3 linker, reduces sensitivity to this process, as prior reports demonstrate that the Kv1.2[T252R] mutant strongly attenuates cell-to-cell variability of Kv1.2 activation (Baronas et al., 2015; Rezazadeh et al., 2007). We used the Kv1.2[T252R] mutant in several experiments, to avoid confounding effects of this poorly understood regulatory mechanism. Coexpression of Kv1.2[T252R] with Kvβ produced a slightly negative shift in the $V_{1/2}$ of channel activation compared with the channel alone (Fig. 4, A–C). Coexpression of Kv1.2[T252R] with Slc7a5 resulted in a dramatic hyperpolarizing shift of the activation $V_{1/2}$ compared with the channel alone or the Kv1.2/Kvβ complex (Fig. 4, A–C). The Slc7a5-mediated gating shift persisted with the addition of Kvβ (Fig. 4, A–C), demonstrating that Kv1.2 can undergo concurrent modulation by Slc7a5 and Kvβ. Similar effects were also observed for WT Kv1.2 (Fig. S3).

Given the robust effects on channel activation by Slc7a5 in the presence and absence of Kvβ, we aimed to understand the combined effects of these proteins in more detail. We recognized early on that the degree of steady-state N-type inactivation of Kv1.2[T252R] + Kvβ was altered by the presence of Slc7a5 (Fig. 4A, right panels). In this experiment, using the Kv1.2[T252R] mutation is helpful because variable activation kinetics of Kv1.2 can significantly obscure the apparent rate and/or extent of Kvβ-mediated inactivation. Therefore, we focused on collection of inactivation data using the Kv1.2[T252R] mutant. To measure steady-state inactivation, cells were pulsed between +50 and −120 mV in 10-mV increments (−80-mV holding potential) for 1 s followed by a test pulse to +30 mV. Current amplitude was measured at the peak of the +30-mV test pulse (Fig. 5, A and B). Slc7a5 caused a prominent hyperpolarizing shift of steady-state inactivation, as expected based on the previously observed Slc7a5-mediated hyperpolarizing shift of channel activation. More importantly, the extent of Kvβ-induced Kv1.2 inactivation was greater upon coexpression with Slc7a5 (Fig. 5, A and B). This finding suggests that coexpression with Slc7a5 enhances Kv1.2

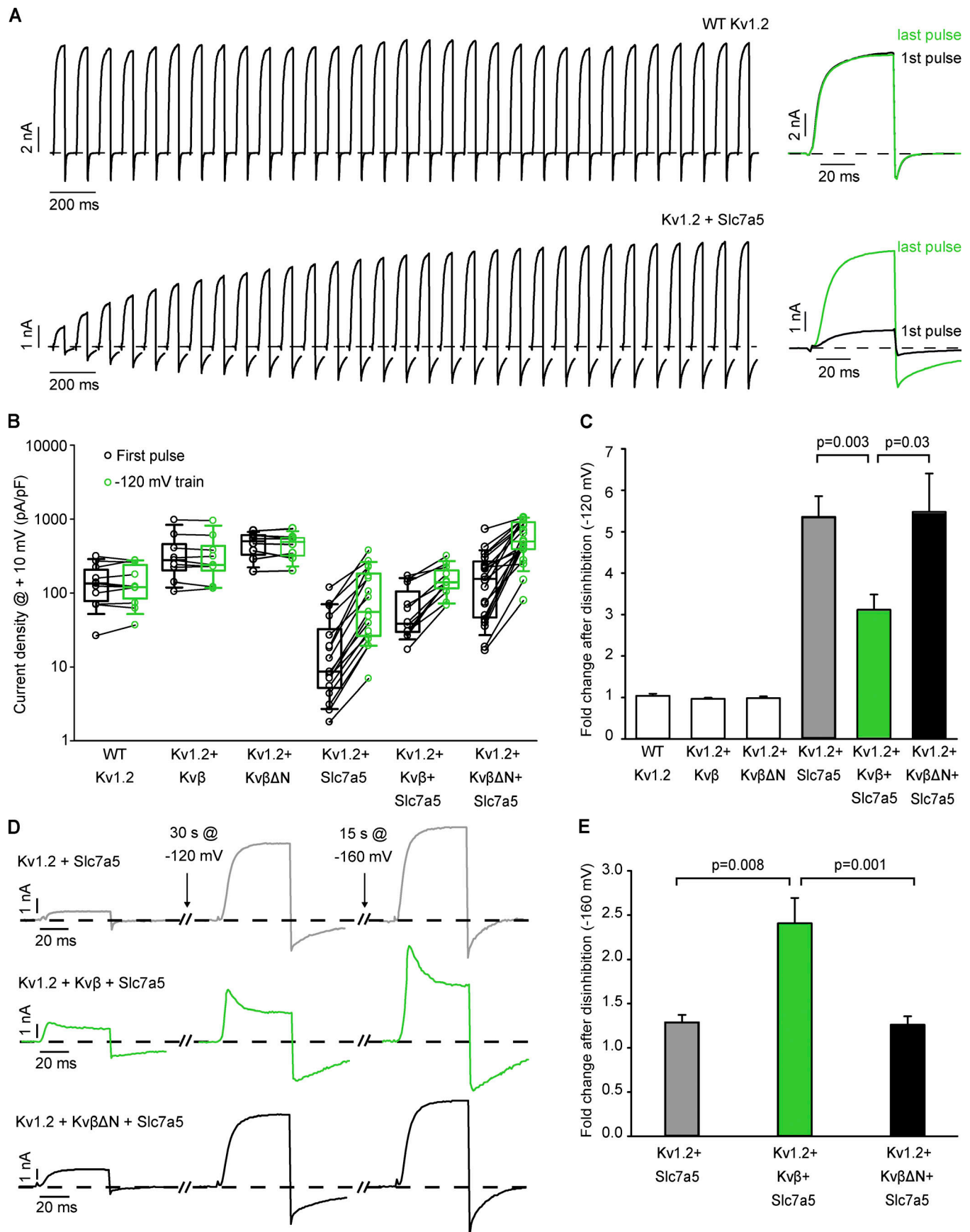


Figure 3. Kv β stabilizes Kv1.2 in an Slc7a5-induced nonconducting state. Combinations (as indicated in Fig. 1A) of WT Kv1.2, Slc7a5, and Kv β or Kv β Δ N were transfected in LM cells. Currents were measured at +10 mV (50-ms pulses, every 2 s). **(A)** Exemplar patch clamp records of WT Kv1.2 and Kv1.2 + Slc7a5 measured continuously at +10 mV (50 ms pulses, every 2 s) from a -120-mV holding voltage. Sample currents on the right depict the peak current amplitude at the first (black) and last (green) pulse following a train of depolarizations from a holding potential of -120 mV. **(B)** Cell-by-cell current density (at +10 mV) of the first pulse (black) and final (green) pulse following a train of depolarizations from a -120-mV holding potential for 30 s ($n = 11$ individual cells recorded for WT Kv1.2, $n = 9$ for Kv1.2 + Kv β , $n = 8$ for Kv1.2 + Kv β Δ N, $n = 16$ for Kv1.2 + Slc7a5, $n = 12$ for Kv1.2 + Kv β + Slc7a5, $n = 20$ for Kv1.2 + Kv β Δ N + Slc7a5). **(C)** Bar graph depicting the mean (\pm SEM) fold change of disinhibition between the first and final test pulses of a 30-s pulse from a -120-mV holding voltage ($n = 11$ for WT Kv1.2, $n = 9$ for Kv1.2 + Kv β , $n = 8$ for Kv1.2 + Kv β Δ N, $n = 16$ for Kv1.2 + Slc7a5, $n = 12$ for Kv1.2 + Kv β + Slc7a5, $n = 20$ for Kv1.2 + Kv β Δ N + Slc7a5). Student's t test was used to compare the fold change of disinhibition of Kv1.2 + Kv β + Slc7a5 versus Kv1.2 + Slc7a5 and Kv1.2 + Kv β Δ N + Slc7a5 versus Kv1.2 + Slc7a5. P values are denoted above the bars. **(D)** Representative traces of the current amplitude following a train of depolarizations from a 30-s holding voltage at -120 mV then an additional 15-s holding voltage at -160 mV. **(E)** Bar graph depicting the mean (\pm SEM) fold change of disinhibition between the first and final test pulses of a 15-s pulse from a -160-mV holding voltage after cells had undergone a 30-s -120-mV train ($n = 6$ for Kv1.2 + Slc7a5, $n = 8$ for Kv1.2 + Kv β + Slc7a5, $n = 15$ for Kv1.2 + Kv β Δ N + Slc7a5). Student's t test was used to compare the fold change of disinhibition of Kv1.2 + Kv β + Slc7a5 versus Kv1.2 + Slc7a5 and Kv1.2 + Kv β Δ N + Slc7a5 versus Kv1.2 + Slc7a5. P values are denoted above the bars.

sensitivity to Kv β -mediated inactivation, so we carried on investigating potential mechanisms.

Slc7a5 influences kinetic features of Kv β -mediated inactivation

We reasoned that effects of Slc7a5 on Kv β -induced inactivation of Kv1.2 might be apparent in various features of channel gating, including the rate of inactivation, recovery from inactivation, or altered deactivation kinetics due to interference of the N-terminal inactivation particle with channel closure. We systematically investigated each of these gating

parameters in the presence or absence of Slc7a5, again using Kv1.2[T252R] + Kv β to minimize the influence of variations in channel activation kinetics. Time constants of inactivation were obtained by fitting inactivating currents with a single exponential function over a range of voltages (Fig. 6A). Coexpression of Slc7a5 with the Kv1.2[T252R] mutant and Kv β caused a modest acceleration of Kv β -mediated inactivation (Fig. 6, A and B). Also, as illustrated in the scaled inactivating current traces at +100 mV (Fig. 6C), the degree of inactivation was greater in the presence of Slc7a5. Similar effects were also observed for WT Kv1.2 (Fig. S4).

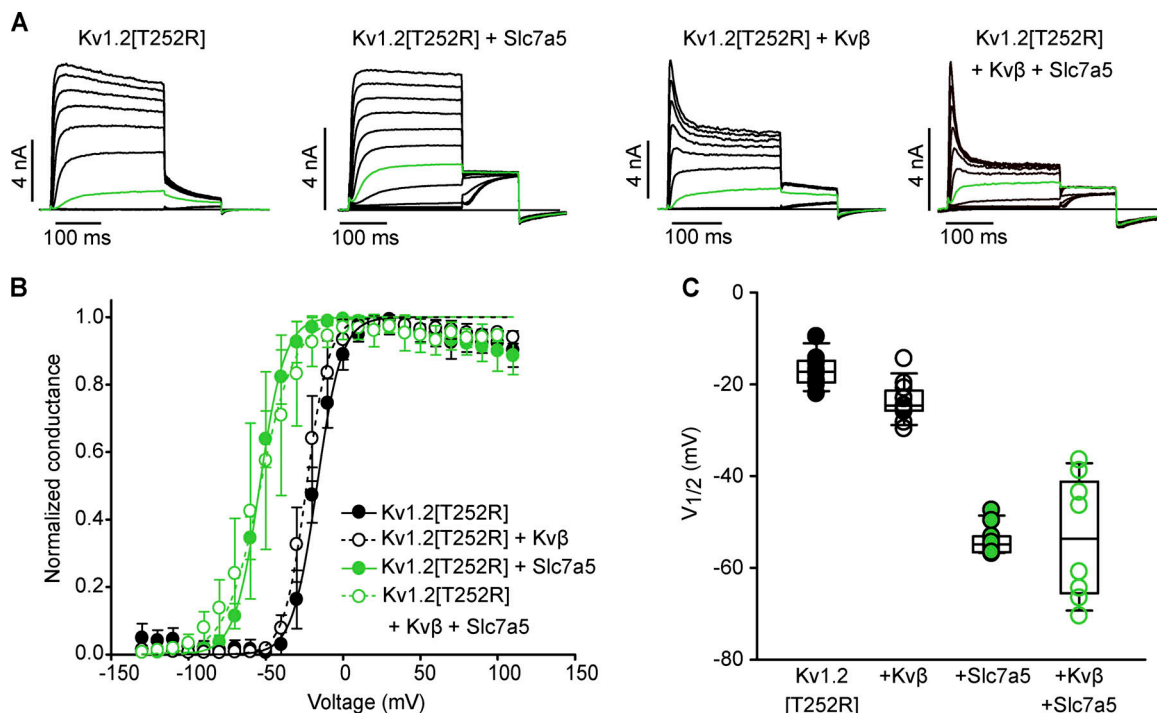


Figure 4. Slc7a5 shifts the voltage dependence of activation of Kv1.2- and Kv β -regulated Kv1.2 channels. **(A)** Combinations (as indicated in Fig. 1A) of Kv1.2[T252R], Slc7a5, and Kv β were transfected in LM cells. Cells were hyperpolarized to -120 mV for 30 s before recording to disinhibit Kv1.2 currents. G-V relationships were measured by stepping between -130 and 110 mV (150 ms in 10-mV steps, -100 mV holding potential) followed by a tail current voltage of -30 mV. Representative current traces of the activation curves with the pulse to -20 mV are highlighted in green. **(B)** G-V plots were generated by analyzing the tail current amplitudes at -30 mV and fitting with a Boltzmann function (Kv1.2[T252R] $V_{1/2} = -16.9 \pm 3.9$ [mean \pm SD], $k = 8.3 \pm 1.9$, $n = 8$ individual cells recorded; Kv1.2[T252R] + Kv β $V_{1/2} = -23.6 \pm 4.2$, $k = 7.5 \pm 1.3$, $n = 11$; Kv1.2[T252R] + Slc7a5 $V_{1/2} = -54 \pm 4$, $k = 8.6 \pm 1.7$, $n = 10$; Kv1.2[T252R] + Kv β + Slc7a5 $V_{1/2} = -54 \pm 14$, $k = 11.7 \pm 1.8$, $n = 8$). **(C)** $V_{1/2}$ of individual cells from each group in A and B are summarized and displayed as box plots for comparison. Box plots depict the median, 25th, and 75th percentiles (box) and the 10th and 90th percentiles (whiskers).

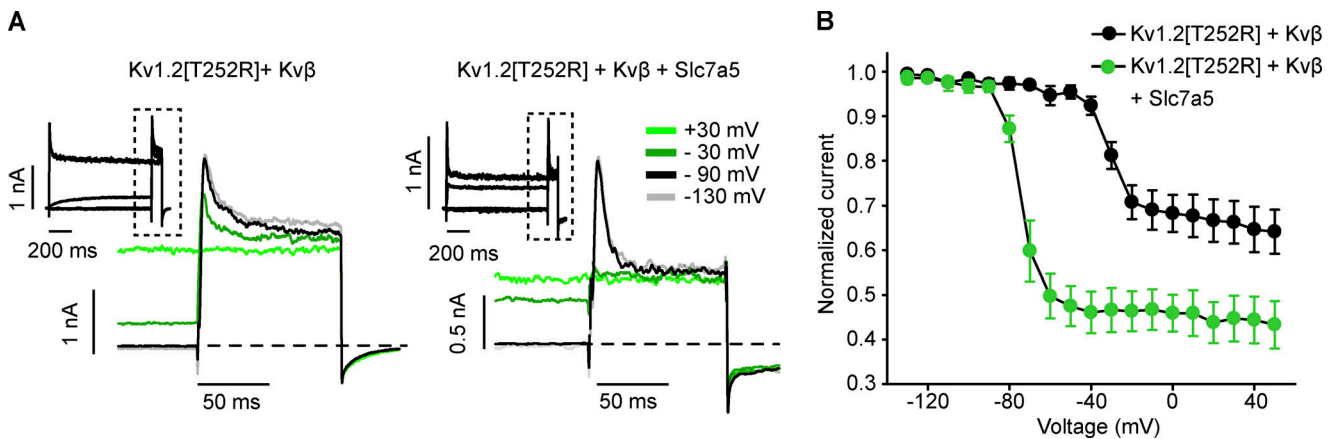


Figure 5. Slc7a5 alters steady-state inactivation of Kvβ-regulated Kv1.2 channels. LM cells were transfected with Kv1.2[T252R] + Kvβ; or Kv1.2[T252R] + Kvβ + Slc7a5 with transfection ratios as previously mentioned. Cells were hyperpolarized to -120 mV for 30 s before recording, to disinhibit Kv1.2 currents. **(A)** Representative current traces of Kv1.2[T252R] + Kvβ and Kv1.2[T252R] + Kvβ + Slc7a5 used to measure the steady-state inactivation plots in B. Magnified insets highlight the test pulse at $+30$ mV from prepulse traces at $+30$, -30 , -90 , and -130 mV. **(B)** Steady-state inactivation of Kv1.2[T252R] + Kvβ and Kv1.2[T252R] + Kvβ + Slc7a5 were measured by stepping from $+50$ to -130 mV in 10-mV increments for 1 s followed by a test pulse to $+30$ mV for 100 ms. Steady-state inactivation plots (mean values ± SEM) were generated by analyzing current amplitudes at the $+30$ -mV test pulse from each prepulse voltage ($n = 5$ individual cells recorded for each group). Box plots depict the median, 25th, and 75th percentiles (box) and the 10th and 90th percentiles (whiskers).

Slc7a5 effects on recovery from inactivation were far more pronounced. To test recovery from N-type inactivation, cells were stepped to $+100$ mV for 500-ms (inactivation step), followed by recovery intervals at various holding potentials for up to 600 ms. Exemplar current traces (Fig. 7 A, -100 -mV recovery potential) illustrate that recovery is markedly slower when Kv1.2[T252R] + Kvβ are coexpressed with Slc7a5. In Kv1.2[T252R] + Kvβ, recovery is nearly complete within 100 ms at a -100 -mV recovery potential. In contrast, Kv1.2[T252R] + Kvβ + Slc7a5 exhibits significant residual inactivation even after

300–400 ms. Summary data illustrate recovery at -100 -mV (Fig. 7 B) and -120 -mV (Fig. 7 C) recovery potentials. With a recovery potential of -120 mV, recovery was faster overall, but the effects of Slc7a5 were still observed.

N-type inactivation influences deactivation by delaying channel closure until the inactivation peptide vacates the pore (England et al., 1995). We examined the interaction of Slc7a5 and Kvβ in the context of Kv1.2 deactivation, by depolarizing cells to $+100$ mV for 200 ms and repolarizing to voltages between -60 to -150 mV for 500 ms in 10-mV increments (Fig. 8 A). WT Kv1.2,

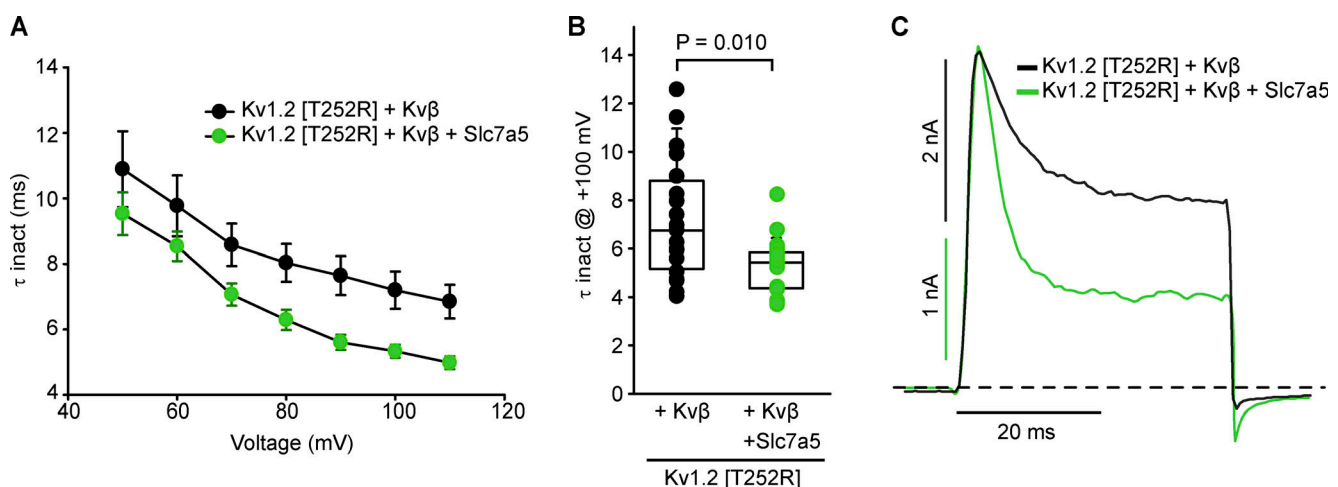


Figure 6. Slc7a5 accelerates Kvβ-mediated N-type inactivation of Kv1.2 channels. LM cells were transfected with Kv1.2[T252R] + Kvβ or Kv1.2[T252R] + Kvβ + Slc7a5 with transfection ratios as previously mentioned. Cells were hyperpolarized to -120 mV for 30 s before recording, to disinhibit Kv1.2 currents. **(A)** Time constants of inactivation (τ_{inact}) were calculated from a single exponential fit of the inactivating current at depolarizing sweeps from 50 to 110 mV in 10-mV increments for 100 ms from a -100 mV holding potential (mean ± SEM) at each voltage ($n = 19$ –20 individual cells recorded for each group). **(B)** τ_{inact} of individual cells from each group in A were obtained from the inactivating currents at $+100$ mV from a -100 -mV holding voltage. τ_{inact} (ms) at $+100$ mV ± SD; Kv1.2[T252R] + Kvβ = 7.2 ± 2.5 ; Kv1.2[T252R] + Kvβ + Slc7a5 = 5.3 ± 1.1 ; $n = 19$ –20 individual cells recorded for each group. Student's *t* test was used to compare the Slc7a5 treatment group versus the respective control; *P* values are denoted above the box plots. **(C)** Representative traces of LM cells were depolarized to $+100$ mV for 40 ms from a -100 -mV holding potential. Box plots depict the median, 25th, and 75th percentiles (box) and the 10th and 90th percentiles (whiskers).

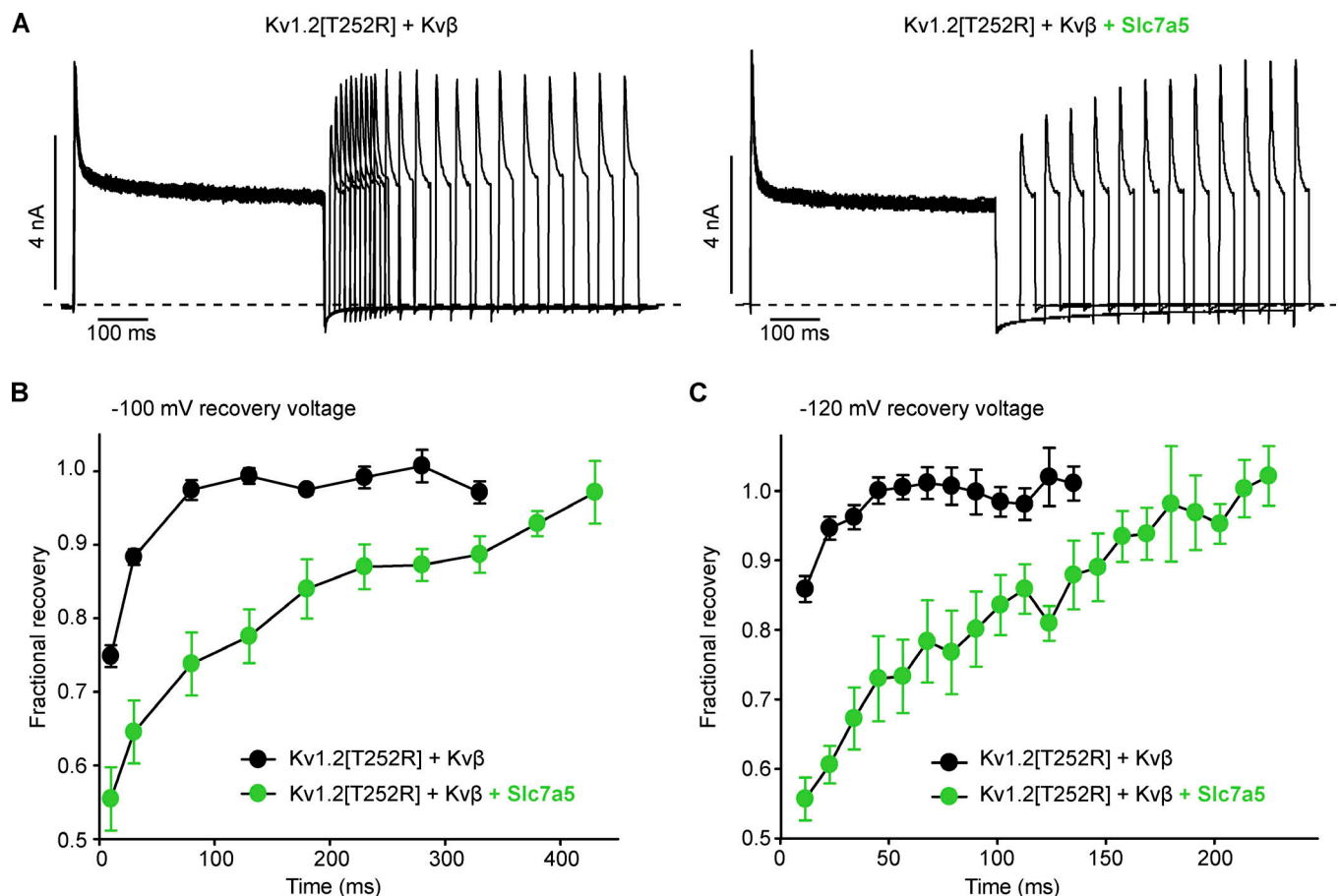


Figure 7. Slc7a5 significantly prolongs recovery from Kvβ-induced inactivation. LM cells expressing Kv1.2[T252R] + Kvβ or Kv1.2[T252R] + Kvβ + Slc7a5 were subjected to 500-ms inactivating pulses to +100 mV followed by repolarizing pulses to -100 mV for 5-, 10-, or 50-ms intervals up to 600 ms. Cells were hyperpolarized to -120 mV for 30 s before recording to disinhibit Kv1.2 currents. **(A)** Representative current traces of channel recovery from inactivation at repolarizing pulses to -100 mV for 10 and/or 50 ms. **(B)** Recovery of the channels from inactivation was measured during 30-ms test pulses to +100 mV, after a -100-mV recovery potential for 5–600 ms. Current amplitude was analyzed at each +100-mV test pulse, following the allotted time at -100 mV (data shown as mean ± SEM, $n = 14$ –16 individual cells recorded for each group). **(C)** Recovery from inactivation was measured during 30-ms test pulses to +100 mV, after a -120 mV recovery potential for 5–600 ms. Current amplitude was analyzed at each +100-mV test pulse, following the allotted time at -120 mV (data shown as mean ± SEM).

Kv1.2 + Kvβ, and Kv1.2 + Slc7a5 deactivation tail currents are well described with a single exponential function (Fig. 8, B and C). In contrast, Kv1.2 + Kvβ + Slc7a5 deactivation tail current exhibited two components (fast and slow; Fig. 8 B). As previously reported, the open-state dependence of Kvβ-mediated inhibition causes modest deceleration of Kv1.2 channel deactivation compared with WT Kv1.2 alone (Fig. 8 C; Accili et al., 1997b). Slc7a5 produced even slower deactivation kinetics compared with Kv1.2 and Kv1.2 + Kvβ across the range of voltages examined (Fig. 8 C) due to the Slc7a5-mediated shift of voltage-dependent gating. Most notably, the Kv1.2 + Kvβ + Slc7a5 condition generated deactivation kinetics that were extremely slow, leading to incomplete channel closure even after 250 ms at -130 mV (Fig. 8 B). The fast component of these tail currents overlapped with the rate of Kv1.2 + Slc7a5 channel (Fig. 8, C and D), suggesting that some channels may not have assembled with both Slc7a5 and Kvβ (Fig. 8 C). The strong initial depolarization to +100 mV did not affect the rates of channel deactivation compared with weaker depolarizing pulses, as

identical results were obtained using a depolarizing pulse to +20 mV instead (Fig. S5).

Kvβ interactions with a gain-of-function Kv1.2 mutant

We sought to confirm that Slc7a5-dependent effects on inactivation and recovery were not secondary consequences of altered channel gating. For example, accelerated activation relative to the inactivation rate could accentuate the apparent extent of inactivation. Similarly, the interaction between deactivation and recovery from N-type inactivation may depend on the relative rates of these processes. Therefore, we tested the effect of Kvβ on a recently reported epilepsy-linked KCNA2 mutation, Kv1.2 [L298F] (Masnada et al., 2017; Syrbe et al., 2015), which causes a hyperpolarizing shift of channel activation by nearly -50 mV (Masnada et al., 2017; Syrbe et al., 2015). This is a useful comparison, because the gating shift is comparable to Slc7a5-mediated actions on Kv1.2, and thus allows us to distinguish Slc7a5-dependent and -independent effects on inactivation parameters.

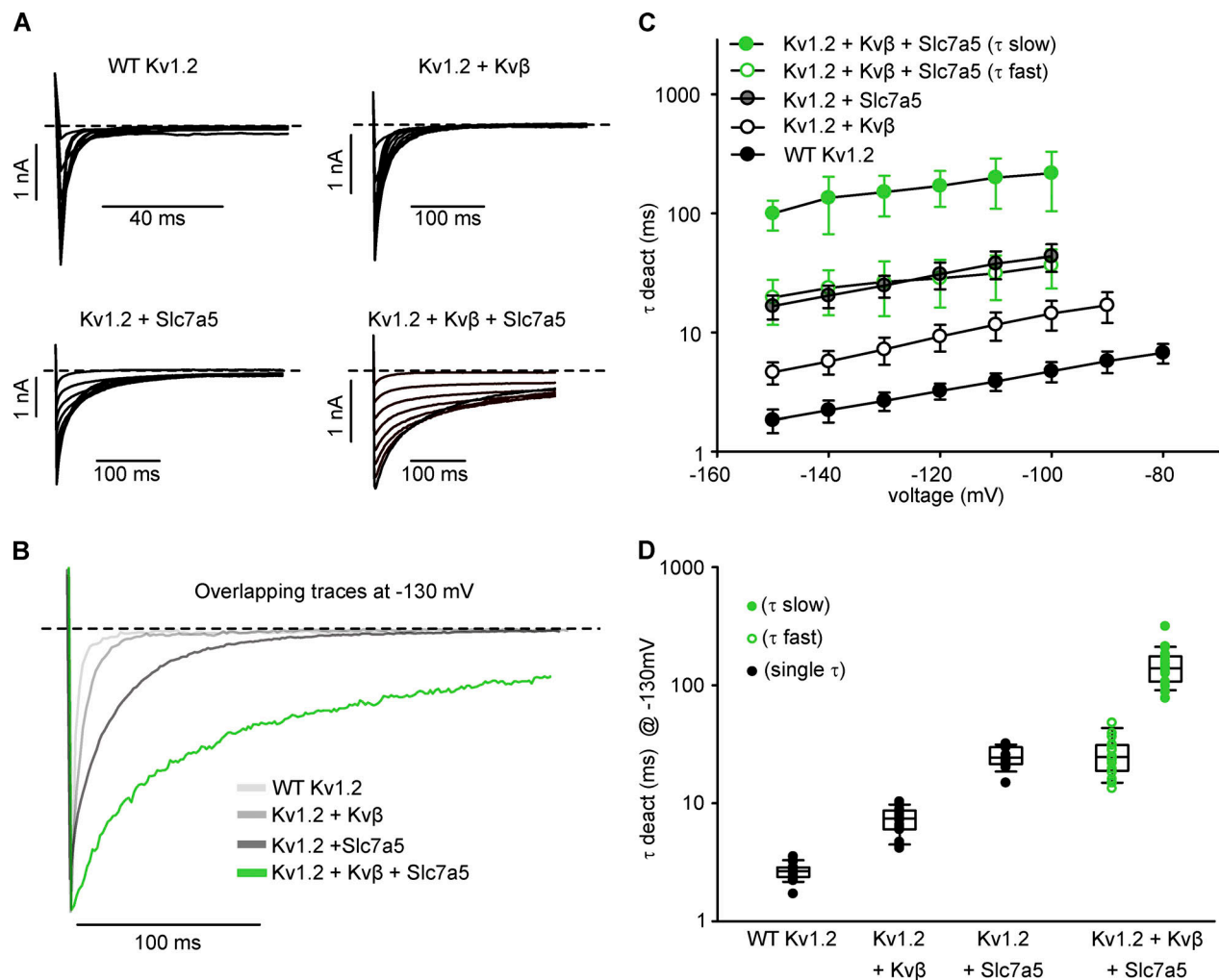


Figure 8. Slc7a5 prolongs deactivation of Kv1.2/Kvβ. (A) Representative current traces of channel deactivation from LM cells transfected with combinations of WT Kv1.2, Kvβ, and Slc7a5. Cells were depolarized to +100 mV for 200 ms followed by repolarizing steps from -60 to -150 mV in 10-mV increments for 600 ms before returning to a -100 mV holding potential. Current traces highlight the deactivation tail currents upon repolarization to voltages between -60 and -150 mV. (B) Overlapping deactivation tail currents at -130 mV from representative current traces in A. Deactivation tails of WT Kv1.2, Kv1.2 + Kvβ, and Kv1.2 + Slc7a5 were fitted with a single exponential function. Deactivation tails of Kv1.2 + Kvβ + Slc7a5 were fitted with a double exponential function. (C) Time constants of deactivation (mean ± SD) calculated from single (WT Kv1.2, Kv1.2 + Kvβ, Kv1.2 + Slc7a5) or double (Kv1.2 + Kvβ + Slc7a5) exponential functions of the deactivation tail currents obtained from the voltage protocol in A. (D) τ Deactivation of individual cells from each group were obtained from the deactivation tail currents at -130 mV from a +100-mV depolarizing step (τ deact [ms] at -130 mV ± SD; WT Kv1.2 = 2.7 ± 0.5; Kv1.2 + Kvβ = 7.2 ± 1.9; Kv1.2 + Slc7a5 = 24.9 ± 5.2; Kv1.2 + Slc7a5 + Kvβ [fast] = 27 ± 13 ms; Kv1.2 + Slc7a5 + Kvβ [slow] = 151 ± 57; n = 13–21 individual cells recorded for each group).

Coexpression of Kv1.2[L298F] with Kvβ produced a rapidly inactivating current with a $V_{1/2}$ that closely resembled the $V_{1/2}$ of Kv1.2[L298F] channel alone (Fig. 9 A) and was shifted slightly in the hyperpolarizing direction compared with Kv1.2[T252R] + Kvβ + Slc7a5 (Fig. 9 B). Although some deceleration of Kv1.2 [L298F] deactivation was observed with Kvβ, the pronounced slow component of deactivation observed for Kv1.2 + Kvβ + Slc7a5 was not apparent (Fig. 9, C and D). Steady-state N-type inactivation and kinetics of inactivation and recovery were tested as described in Figs. 5, 6, and 7. We observed a hyperpolarizing shift in steady-state inactivation, resulting from the negative shift in channel activation of the L298F mutant. More importantly, the extent of inactivation was less than observed for Kv1.2[T252R] + Kvβ + Slc7a5 (Fig. 9 E). Consistent with this, the rate of inactivation of Kv1.2[L298F] + Kvβ was similar to that

of Kv1.2[T252R] + Kvβ and did not display the acceleration observed when Kv1.2[T252R] is coexpressed with Slc7a5 (Fig. 9 F). Lastly, we analyzed recovery of the Kv1.2[L298F] + Kvβ channel from inactivation. The rate of recovery from inactivation closely resembled the Kv1.2[T252R] + Kvβ control (Fig. 9 G). These findings suggest that the observed stabilization of N-type inactivation by Slc7a5 is not an indirect consequence of the shift in activation gating, but rather is a distinct functional outcome of Slc7a5 on the channel-Kvβ complex.

Discussion

Molecular mechanisms of Kv channel gating have been studied in fine detail, but less is known about regulatory proteins that may influence maturation or gating of many Kv channel

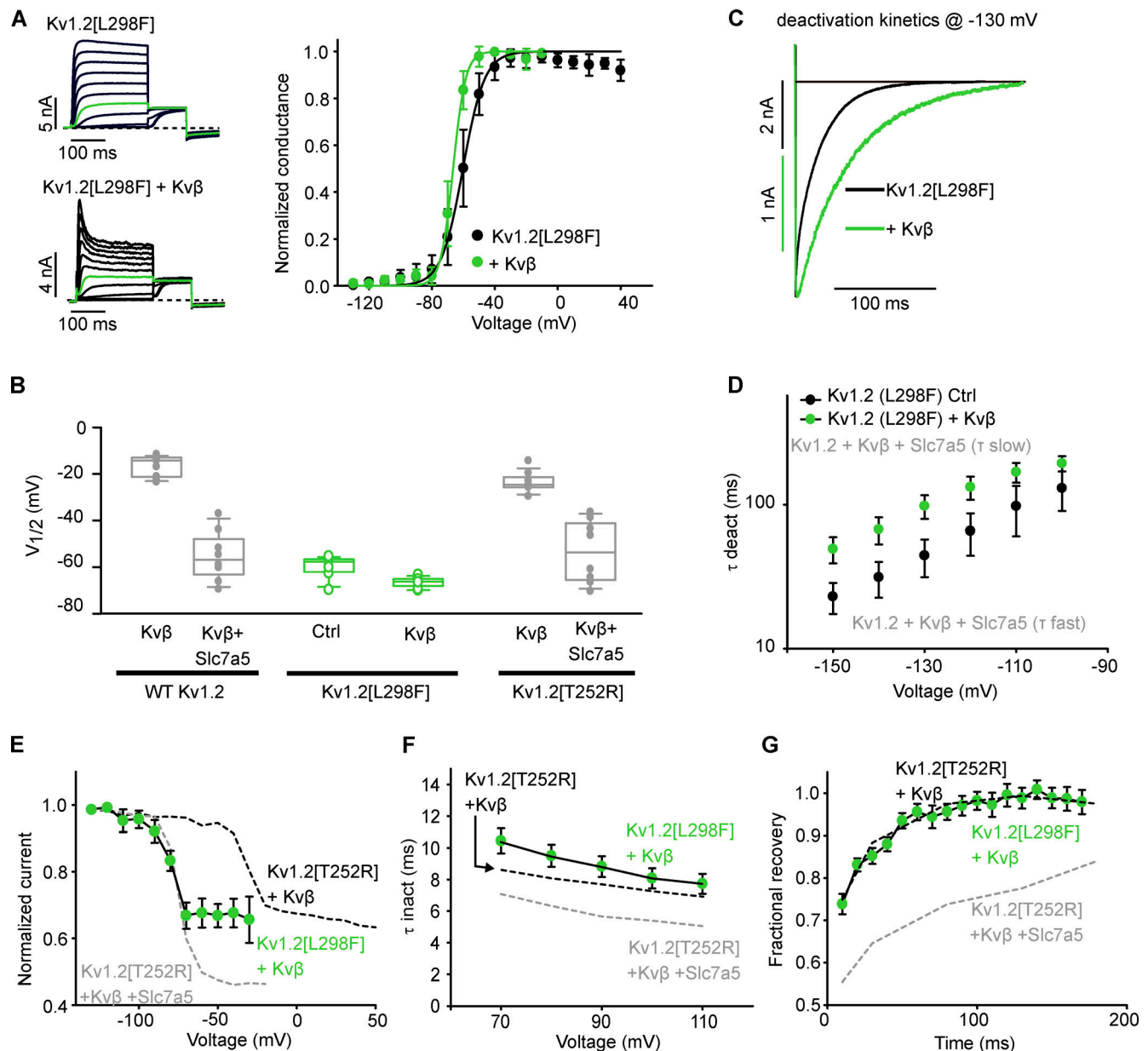


Figure 9. Regulation of Kv1.2[L298F] by Kvβ. (A) LM cells were transfected with Kv1.2[L298F] in the absence or presence of Kvβ. Left: Representative current traces of the activation curves, with the pulse to -20 mV highlighted in green. Right: G-V relationships were measured as described in Fig. 3 A. G-V relationships were generated from the tail current amplitudes and fitted with a Boltzmann function. Kv1.2[L298F] $V_{1/2}$ = -60 ± 5 (mean ± SD), k = 7.2 ± 1.6, n = 10 individual cells recorded; Kv1.2[L298F] + Kvβ $V_{1/2}$ = -66.6 ± 2.3, k = 4.1 ± 0.6, n = 8. (B) $V_{1/2}$ of individual cells from Kv1.2[L298F] and Kv1.2[L298F] + Kvβ (green) along with select $V_{1/2}$ values from Fig. 1 and Fig. S1 (gray). (C) Overlapping deactivation tail currents of Kv1.2[L298F] and Kv1.2[L298F] + Kvβ at -130 mV from a +100-mV depolarizing voltage. Deactivation tails of Kv1.2[L298F] and Kv1.2[L298F] + Kvβ were fitted with a single exponential function. (D) Time constants of deactivation (τ_{deact} at -130 mV) calculated from single exponential functions of the deactivation tail currents of Kv1.2[L298F] and Kv1.2[L298F] + Kvβ obtained using the voltage protocol described in Fig. 7 A (mean ± SD; Kv1.2[L298F] Ctrl = 44 ± 13 ms, Kv1.2[L298F] + Kvβ = 98 ± 18 ms; n = 12–13 individual cells recorded for each group). (E) Steady-state inactivation plots of Kv1.2[L298F] + Kvβ were generated using the voltage protocol described in Fig. 4 A (n = 7 individual cells recorded). Data from Fig. 4 D are superimposed for comparison. (F) Time constants of inactivation (at +100 mV) were calculated using the voltage protocol described in Fig. 5 A (mean ± SD; Kv1.2[L298F] + Kvβ = 8.0 ± 2.8 ms; n = 19 individual cells recorded). Data from Fig. 5 A are superimposed for comparison (black dotted lines). (G) Recovery from inactivation was measured using the voltage protocol described in Fig. 6 A (n = 11 individual cells recorded). Data from Fig. 6 A are superimposed for comparison (black dotted lines). Box plots depict the median, 25th, and 75th percentiles (box) and the 10th and 90th percentiles (whiskers).

subtypes. A small number of well-known regulatory proteins including the Kvβ subunits have been studied, but we suspect that regulatory proteins encountered by many Kv channel types during their maturation or normal function remain unknown.

We recently reported powerful effects of Slc7a5 on gating and expression of Kv1.2 channels, and in this study, we have extended this work to consider the possibility that Slc7a5 and other subunits such as Kvβ can coregulate ion channels and generate

distinct functional properties. This detailed study should be considered in the broader context of whether, where, and how Kv channels might assemble into multiprotein complexes.

We report that coexpression of Kv1.2 with Kv β and Slc7a5 leads to a combination of hallmark features of both regulatory proteins, including Kv β -mediated rapid inactivation (Fig. 1), Slc7a5-mediated disinhibition (Fig. 3), and shift in voltage-dependence of activation (Fig. 4). These proteins also appear to interact at the level of Kv1.2 proteostasis, as Kv β partly counteracts Slc7a5-mediated reduction of Kv1.2 current and protein expression (Figs. 1 and 3). We focused primarily on the gating effects arising from coexpression of Slc7a5 and Kv β , most notably the combination of a shift in the voltage dependence and extent of inactivation. Based on our characterization of multiple gating parameters, more pronounced Kv β -mediated inactivation in the presence of Slc7a5 is predominantly due to deceleration of recovery from inactivation (Fig. 7), although a modest acceleration of inactivation was also observed (Fig. 6).

A direct association between Kv β and Kv1.2 is well established, but it is not yet clear what molecular mechanism might underlie Slc7a5 modulation. Our previous study used a bioluminescence resonance energy transfer approach to demonstrate close proximity of Slc7a5 and Kv1.2 when overexpressed in cell lines, but it has not been definitively demonstrated whether they interact directly or via an intermediary (Baronas et al., 2018). An Slc7a5-mediated suppression of mature and immature Kv1.2 may suggest that Kv1.2 interacts early in the biosynthetic pathway with Slc7a5, limiting the maturation and trafficking of channels to the cell surface. The transmembrane architecture of Slc7a5 may permit association with Kv1.2 along with Kv β , which is known to assemble with the cytoplasmic T1 domain (Gulbis et al., 2000; Yan et al., 2019). Co-IP experiments support the notion that Kv β and Slc7a5 do not compete for interaction with Kv1.2 since we observed an association between Kv1.2 and Kv β in the presence of Slc7a5 (Fig. 2). Another possibility is that Slc7a5 is coupled to mTOR activation via amino acid transport, and although there are no amino acid substrates of Slc7a5 in our recording solutions, it is possible that overexpression of Slc7a5 leads to persistent activation of pathways that regulate Kv1.2 (Nicklin et al., 2009). Whether the effects of Slc7a5 are mediated by a direct interaction or an indirect mechanism, our findings suggest that Slc7a5 influences Kv1.2 by stabilizing binding of the Kv β N-terminal ball-and-chain peptide to the pore, reflected in a slow rate of dissociation/recovery from inactivation (Fig. 10).

An important consideration for our study is the relative abundance of transfected constructs in our system. While Kv β has been reported to assemble with Kv1.2 with 1:1 stoichiometry (Gulbis et al., 1999), other reports have suggested that substoichiometric assembly with Kv1.2 may occur depending on the relative concentration of Kv α to Kv β subunits (Xu et al., 1998). It has been common to include an excess of Kv β , possibly to ensure stoichiometric assembly with the channel. For example, previous reports have used Kv β in *Xenopus laevis* oocytes with a 1:50 (Kv1.2:Kv β) injection ratio (Accili et al., 1997b). Additionally, assembly of Kv β 1.2 inactivating subunits with endogenous noninactivating Kv β 2 subunits in our expression system may

influence the inactivation kinetics observed in our study (Accili et al., 1997a). We consistently coexpressed proteins at a ratio of 1:4:0.5 (Kv1.2:Kv β :Slc7a5). The amount of Kv β expressed in the cells with a 1:4 (Kv1.2[T252R]:Kv β) transfection ratio appears to cause a saturating effect, since increasing the abundance of Kv β with a 1:10 (Kv1.2[T252R]:Kv β) transfection ratio does not accelerate the rate of inactivation (Fig. S6). Furthermore, a transfection ratio of 1:10:0.5 (Kv1.2[T252R]:Kv β :Slc7a5) did not accelerate the rate of inactivation compared with the 1:4:0.5 condition (Fig. 6, Fig. S4, and Fig. S6). A transfection ratio of 1:0.5 (Kv1.2:Slc7a5) was used in our previous study (Baronas et al., 2018) which was sufficient to observe the hyperpolarizing gating shift and current suppression as reported in this study.

Previous work demonstrated that Slc7a5 contributes to current suppression by forcing Kv1.2 channels into a nonconducting state, which can be reversed (or disinhibited) with negative holding potentials (Baronas et al., 2018). This nonconducting state may be related to C-type inactivation, as we previously reported that Slc7a5 markedly accelerated inactivation of Kv1.2 [V381T], which makes Kv1.2 channels more susceptible to C-type inactivation (Baronas et al., 2018). In channels prone to C-type inactivation, N-type inactivation accelerates C-type (Baukrowitz and Yellen, 1995; Rasmusson et al., 1995; Kurata et al., 2004). This phenomenon may be related to the stronger negative holding voltages required for full disinhibition of channels cotransfected with Kv β and Slc7a5 (Fig. 3). Additionally, these effects may contribute to the Slc7a5-mediated changes in recovery from inactivation we have observed (Fig. 7). C-type inactivation becomes apparent during recovery from inactivation, where it becomes a rate-limiting step for recovery and masks the unbinding kinetics of the inactivation ball peptide (Rasmusson et al., 1995; Morales et al., 1996). Similarly, in our experiments, the Slc7a5-dependent deceleration of recovery from inactivation may reflect an inactivated conformation that is stabilized by Slc7a5 (Fig. 7).

Identification of unique characteristics arising from coregulation of Kv1.2 by Kv β and Slc7a5 may have important implications for understanding the diversity of regulatory mechanisms of Kv channels and potential molecular architecture of A-type currents. Transient inactivating A-type currents (I_A) are prominent K⁺ currents in the central nervous system (Rudy et al., 1988; Bardoni and Belluzzi, 1993; Kanold and Manis, 1999) that activate and inactivate at subthreshold action potential voltages, typically between −45 and −60 mV, and inactivate rapidly during depolarization (Song, 2002; Amberg et al., 2003). In the central nervous system, the major components of I_A are believed to be controlled predominantly by Kv4 subunits, in complex with accessory proteins DPP (dipeptidyl aminopeptidase-like protein) and KChIP (Kv channel interacting protein; Tsaur et al., 1997; Serôdio and Rudy, 1998; Shibata et al., 2000; Chen et al., 2006; Jerng and Pfaffinger, 2014). However, the variability in inactivation kinetics (e.g., time constant, steady state, and recovery) observed in different neuronal cells are unlikely to be explained by a single Kv channel subtype (Bouskila and Dudek, 1995; Connor and Stevens, 1971; Ruben and Thompson, 1984; Rudy, 1988). In this regard, Kv1 subfamilies that interact with the Kv β subunits confer A-type properties

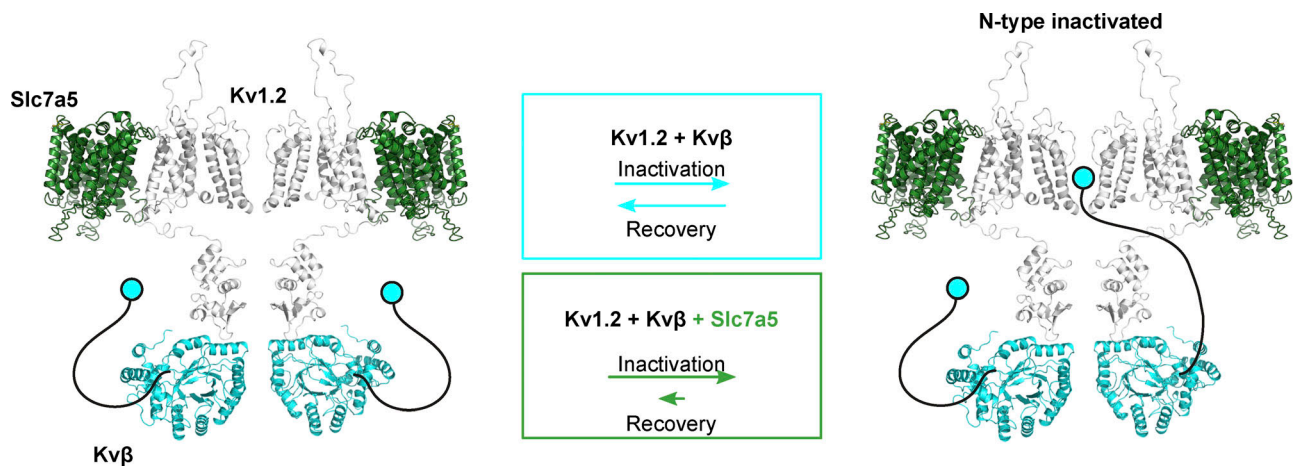


Figure 10. **Graphical summary of Slc7a5 effects on Kvβ-mediated N-type inactivation.** Schematic model depicting hypothetical orientations and interactions of Kv1.2 (gray), Kvβ (light blue), and Slc7a5 (green). The N-terminal ball-and-chain peptide of the Kvβ subunit, which confers N-type inactivation of Kv1.2, is depicted as a cartoon (black and blue) for visualization purposes. We observed that Slc7a5 promotes an interaction between Kv1.2 and Kvβ, and we propose that Slc7a5 primarily alters unbinding of the Kvβ inactivation peptide from the pore of Kv1.2, illustrated by the different relative rates in the colored boxes. The Kv1.2/Kvβ/Slc7a5 complex favors an inactivated state, reflected in a modest acceleration of inactivation and more prominently delayed recovery from inactivation compared with Kv1.2/Kvβ alone.

(Rettig et al., 1994). Our findings suggest that the Kv1.2/Kvβ/Slc7a5 system, displaying rapid inactivation time constants (Fig. 6) and a hyperpolarized $V_{1/2}$ (Fig. 4), possesses properties of I_A and could contribute to A-type currents in neuronal cells that express Kv1.2 and Kvβ1 or Kvβ3 isoforms. Although we have previously demonstrated coexpression of Kv1.2 and Slc7a5 in dissociated cortical and hippocampal neurons (Baronas et al., 2018), there has not been a specific native neuronal current assigned to this channel:transporter architecture, or a larger Kv1.2/Kvβ/Slc7a5 complex. Other Slc7 subtypes and other Kv1 subtypes are currently under investigation to determine how common this category of interaction may be. Publicly available data (e.g., mousebrain.org and neuroseq.janelia.org) report co-expression of Kv1, Kvβ, and various Slc7 subtypes using single-cell RNA sequencing, although the most significant interactions are not currently known, because channel and transporter transcripts are often of low abundance.

The rate of recovery from inactivation is a feature that distinguishes various A-type currents. While Kv4α subunits have rapid recoveries (time constant < 100 ms), A-type currents displaying considerably slower time constants of recovery from inactivation (0.8–1 s) have been suggested to be mediated by Kv1 channels, although a range of recovery rates has been observed (Amberg et al., 2003). This is in line with our observations in Fig. 7, demonstrating that while Kv1.2/Kvβ have relatively fast inactivation time constants, Slc7a5 delays recovery of the complex. Recognition of slower time constants of recovery caused by a Kv1.2/Kvβ/Slc7a5 channel complex, in combination with faster rates of recovery by Kv4 or other Kv subtypes, would help categorize neurons with A-type currents that display both fast and slow components of recovery from inactivation.

In summary, we report the properties of a channel complex involving simultaneous regulation of Kv1.2 gating by cytoplasmic regulatory Kvβ subunits and the transmembrane amino acid transporter, Slc7a5. Functional interactions between these

proteins highlights the importance for continued investigation of novel Kv channel regulatory subunits.

Acknowledgments

Merritt C. Maduke served as editor.

This work was funded by a Canadian Institutes of Health Research Project Grant to H.T. Kurata (CIHR PS148815). S.M. Lamothe was supported by a Rowland and Muriel Haryett Fellowship, University of Alberta Neuroscience and Mental Health Institute. H.T. Kurata was supported by a Canadian Institutes of Health Research Early Career Investigator award and salary support from the Alberta Diabetes Institute.

The authors declare no competing financial interest.

Author contributions: S.M. Lamothe and H.T. Kurata designed the experiments. S.M. Lamothe performed the experiments. S.M. Lamothe analyzed the data. S.M. Lamothe and H.T. Kurata wrote the manuscript. S.M. Lamothe and H.T. Kurata edited and approved the final version.

Submitted: 30 October 2019

Revised: 22 January 2020

Accepted: 13 March 2020

References

- Accili, E.A., J. Kiehn, B.A. Wible, and A.M. Brown. 1997a. Interactions among inactivating and noninactivating Kvβ subunits, and Kvalpha1.2, produce potassium currents with intermediate inactivation. *J. Biol. Chem.* 272:28232–28236. <https://doi.org/10.1074/jbc.272.45.28232>
- Accili, E.A., J. Kiehn, Q. Yang, Z. Wang, A.M. Brown, and B.A. Wible. 1997b. Separable Kvβ subunit domains alter expression and gating of potassium channels. *J. Biol. Chem.* 272:25824–25831. <https://doi.org/10.1074/jbc.272.41.25824>
- Allen, N.M., J. Conroy, A. Shahwan, B. Lynch, R.G. Correa, S.D.J. Pena, D. McCreary, T.R. Magalhães, S. Ennis, S.A. Lynch, and M.D. King. 2016. Unexplained early onset epileptic encephalopathy: Exome screening

- and phenotype expansion. *Epilepsia*. 57:e12–e17. <https://doi.org/10.1111/epi.13250>
- Amberg, G.C., S.D. Koh, Y. Imaizumi, S. Ohya, and K.M. Sanders. 2003. A-type potassium currents in smooth muscle. *Am. J. Physiol. Cell Physiol.* 284:C583–C595. <https://doi.org/10.1152/ajpcell.00301.2002>
- Bardoni, R., and O. Belluzzi. 1993. Kinetic study and numerical reconstruction of A-type current in granule cells of rat cerebellar slices. *J. Neurophysiol.* 69:2222–2231. <https://doi.org/10.1152/jn.1993.69.6.2222>
- Baronas, V.A., B.R. McGuinness, G.S. Brigidi, R.N. Gomm Kolisko, Y.Y. Vilin, R.Y. Kim, F.C. Lynn, S.X. Bamji, R. Yang, and H.T. Kurata. 2015. Use-dependent activation of neuronal Kv1.2 channel complexes. *J. Neurosci.* 35:3515–3524. <https://doi.org/10.1523/JNEUROSCI.4518-13.2015>
- Baronas, V.A., R.Y. Yang, and H.T. Kurata. 2017. Extracellular redox sensitivity of Kv1.2 potassium channels. *Sci. Rep.* 7:9142. <https://doi.org/10.1038/s41598-017-08718-z>
- Baronas, V.A., R.Y. Yang, L.C. Morales, S. Sipione, and H.T. Kurata. 2018. Slc7a5 regulates Kv1.2 channels and modifies functional outcomes of epilepsy-linked channel mutations. *Nat. Commun.* 9:4417. <https://doi.org/10.1038/s41467-018-06859-x>
- Baukrowitz, T., and G. Yellen. 1995. Modulation of K⁺ current by frequency and external [K⁺]: a tale of two inactivation mechanisms. *Neuron*. 15: 951–960. [https://doi.org/10.1016/0896-6273\(95\)90185-X](https://doi.org/10.1016/0896-6273(95)90185-X)
- Bean, B.P. 2007. The action potential in mammalian central neurons. *Nat. Rev. Neurosci.* 8:451–465. <https://doi.org/10.1038/nrn2148>
- Bekkers, J.M., and A.J. Delaney. 2001. Modulation of excitability by alpha-dendrotoxin-sensitive potassium channels in neocortical pyramidal neurons. *J. Neurosci.* 21:6553–6560. <https://doi.org/10.1523/JNEUROSCI.21-17-06553.2001>
- Bouskila, Y., and F.E. Dudek. 1995. A rapidly activating type of outward rectifier K⁺ current and A-current in rat suprachiasmatic nucleus neurones. *J. Physiol.* 488:339–350. <https://doi.org/10.1113/jphysiol.1995.sp020970>
- Cachero, T.G., A.D. Morielli, and E.G. Peralta. 1998. The small GTP-binding protein RhoA regulates a delayed rectifier potassium channel. *Cell*. 93: 1077–1085. [https://doi.org/10.1016/S0092-8674\(00\)81212-X](https://doi.org/10.1016/S0092-8674(00)81212-X)
- Chen, X., L.-L. Yuan, C. Zhao, S.G. Birnbaum, A. Frick, W.E. Jung, T.L. Schwarz, J.D. Sweatt, and D. Johnston. 2006. Deletion of Kv4.2 gene eliminates dendritic A-type K⁺ current and enhances induction of long-term potentiation in hippocampal CA1 pyramidal neurons. *J. Neurosci.* 26:12143–12151. <https://doi.org/10.1523/JNEUROSCI.2667-06.2006>
- Connor, J.A., and C.F. Stevens. 1971. Voltage clamp studies of a transient outward membrane current in gastropod neural somata. *J. Physiol.* 213: 21–30. <https://doi.org/10.1113/jphysiol.1971.sp009365>
- Connor, J.X., K. McCormack, A. Pletsch, S. Gaeta, B. Ganetzky, S.-Y. Chiu, and A. Messing. 2005. Genetic modifiers of the Kv beta2-null phenotype in mice. *Genes Brain Behav.* 4:77–88. <https://doi.org/10.1111/j.1601-183X.2004.00094.x>
- Corbett, M.A., S.T. Bellows, M. Li, R. Carroll, S. Micallef, G.L. Carvill, C.T. Myers, K.B. Howell, S. Maljevic, H. Lerche, et al. 2016. Dominant KCNA2 mutation causes episodic ataxia and pharmacoresponsive epilepsy. *Neurology*. 87: 1975–1984. <https://doi.org/10.1212/WNL.0000000000003309>
- England, S.K., V.N. Uebele, H. Shear, J. Kodali, P.B. Bennett, and M.M. Tamkun. 1995. Characterization of a voltage-gated K⁺ channel beta subunit expressed in human heart. *Proc. Natl. Acad. Sci. USA*. 92: 6309–6313. <https://doi.org/10.1073/pnas.92.14.6309>
- Fogle, K.J., L.S. Baik, J.H. Houl, T.T. Tran, L. Roberts, N.A. Dahm, Y. Cao, M. Zhou, and T.C. Holmes. 2015. CRYPTOCHROME-mediated photo-transduction by modulation of the potassium ion channel β -subunit redox sensor. *Proc. Natl. Acad. Sci. USA*. 112:2245–2250. <https://doi.org/10.1073/pnas.1416586112>
- Giese, K.P., J.F. Storm, D. Reuter, N.B. Fedorov, L.R. Shao, T. Leicher, O. Pongs, and A.J. Silva. 1998. Reduced K⁺ channel inactivation, spike broadening, and after-hyperpolarization in Kvbeta1.1-deficient mice with impaired learning. *Learn. Mem.* 5:257–273.
- Grissmer, S., A.N. Nguyen, J. Aiyar, D.C. Hanson, R.J. Mather, G.A. Gutman, M.J. Kamilowicz, D.D. Auferin, and K.G. Chandy. 1994. Pharmacological characterization of five cloned voltage-gated K⁺ channels, types Kv1.1, 1.2, 1.3, 1.5, and 3.1, stably expressed in mammalian cell lines. *Mol. Pharmacol.* 45:1227–1234.
- Gu, C., Y.N. Jan, and L.Y. Jan. 2003. A conserved domain in axonal targeting of Kv1 (Shaker) voltage-gated potassium channels. *Science*. 301:646–649. <https://doi.org/10.1126/science.1086998>
- Guan, D., J.C.F. Lee, M.H. Higgs, W.J. Spain, and R.C. Foehring. 2007. Functional roles of Kv1 channels in neocortical pyramidal neurons. *J. Neurophysiol.* 97:1931–1940. <https://doi.org/10.1152/jn.00933.2006>
- Gulbis, J.M., S. Mann, and R. MacKinnon. 1999. Structure of a voltage-dependent K⁺ channel beta subunit. *Cell*. 97:943–952. [https://doi.org/10.1016/S0092-8674\(00\)80805-3](https://doi.org/10.1016/S0092-8674(00)80805-3)
- Gulbis, J.M., M. Zhou, S. Mann, and R. MacKinnon. 2000. Structure of the cytoplasmic beta subunit-T1 assembly of voltage-dependent K⁺ channels. *Science*. 289:123–127. <https://doi.org/10.1126/science.289.5476.123>
- Heinemann, S.H., J. Rettig, F. Wunder, and O. Pongs. 1995. Molecular and functional characterization of a rat brain Kv beta 3 potassium channel subunit. *FEBS Lett.* 377:383–389. [https://doi.org/10.1016/0014-5793\(95\)01377-6](https://doi.org/10.1016/0014-5793(95)01377-6)
- Hite, R.K., J.A. Butterwick, and R. MacKinnon. 2014. Phosphatidic acid modulation of Kv channel voltage sensor function. *eLife*. 3:e04366. <https://doi.org/10.7554/eLife.04366>
- Ho, S.N., H.D. Hunt, R.M. Horton, J.K. Pullen, and L.R. Pease. 1989. Site-directed mutagenesis by overlap extension using the polymerase chain reaction. *Gene*. 77:51–59. [https://doi.org/10.1016/0378-1119\(89\)90358-2](https://doi.org/10.1016/0378-1119(89)90358-2)
- Ishikawa, K., M. Tanaka, J.A. Black, and S.G. Waxman. 1999. Changes in expression of voltage-gated potassium channels in dorsal root ganglion neurons following axotomy. *Muscle Nerve*. 22:502–507. [https://doi.org/10.1002/\(SICI\)1097-4598\(199904\)22:4<502::AID-MUS12>3.0.CO;2-K](https://doi.org/10.1002/(SICI)1097-4598(199904)22:4<502::AID-MUS12>3.0.CO;2-K)
- Jerng, H.H., and P.J. Pfaffinger. 2014. Modulatory mechanisms and multiple functions of somatodendritic A-type K⁺ channel auxiliary subunits. *Front. Cell. Neurosci.* 8:82. <https://doi.org/10.3389/fncel.2014.00082>
- Kanold, P.O., and P.B. Manis. 1999. Transient potassium currents regulate the discharge patterns of dorsal cochlear nucleus pyramidal cells. *J. Neurosci.* 19:2195–2208. <https://doi.org/10.1523/JNEUROSCI.19-06-02195.1999>
- Kempf, A., S.M. Song, C.B. Talbot, and G. Miesenböck. 2019. A potassium channel β -subunit couples mitochondrial electron transport to sleep. *Nature*. 568:230–234. <https://doi.org/10.1038/s41586-019-1034-5>
- Kobertz, W.R., C. Williams, and C. Miller. 2000. Hanging gondola structure of the T1 domain in a voltage-gated K⁺ channel. *Biochemistry*. 39: 10347–10352. <https://doi.org/10.1021/bi001292j>
- Kourrich, S., T. Hayashi, J.-Y. Chuang, S.-Y. Tsai, T.-P. Su, and A. Bonci. 2013. Dynamic interaction between sigma-1 receptor and Kv1.2 shapes neuronal and behavioral responses to cocaine. *Cell*. 152:236–247. <https://doi.org/10.1016/j.cell.2012.12.004>
- Kruse, M., and B. Hille. 2013. The phosphoinositide sensitivity of the K(v) channel family. *Channels (Austin)*. 7:530–536. <https://doi.org/10.4161/chan.25816>
- Kurata, H.T., Z. Wang, and D. Fedida. 2004. NH₂-terminal inactivation peptide binding to C-type-inactivated Kv channels. *J. Gen. Physiol.* 123: 505–520. <https://doi.org/10.1085/jgp.200308956>
- Li, D., K. Takimoto, and E.S. Levitan. 2000. Surface expression of Kv1 channels is governed by a C-terminal motif. *J. Biol. Chem.* 275: 11597–11602. <https://doi.org/10.1074/jbc.275.16.11597>
- Long, S.B., E.B. Campbell, and R. MacKinnon. 2005. Crystal structure of a mammalian voltage-dependent Shaker family K⁺ channel. *Science*. 309: 897–903. <https://doi.org/10.1126/science.1116269>
- Masnada, S., U.B.S. Hedrich, E. Gardella, J. Schubert, C. Kaiwar, E.W. Klee, B.C. Lanpher, R.H. Gavrilo, M. Synofzik, T. Bast, et al. 2017. Clinical spectrum and genotype-phenotype associations of KCNA2-related encephalopathies. *Brain*. 140:2337–2354. <https://doi.org/10.1093/brain/awx184>
- McCormack, K., J.X. Connor, L. Zhou, L.L. Ho, B. Ganetzky, S.-Y. Chiu, and A. Messing. 2002. Genetic analysis of the mammalian K⁺ channel beta subunit Kvbeta 2 (Kcnab2). *J. Biol. Chem.* 277:13219–13228. <https://doi.org/10.1074/jbc.M111465200>
- Morales, M.J., J.O. Wee, S. Wang, H.C. Strauss, and R.L. Rasmusson. 1996. The N-terminal domain of a K⁺ channel beta subunit increases the rate of C-type inactivation from the cytoplasmic side of the channel. *Proc. Natl. Acad. Sci. USA*. 93:15119–15123. <https://doi.org/10.1073/pnas.93.26.15119>
- Nesti, E., B. Everill, and A.D. Morielli. 2004. Endocytosis as a mechanism for tyrosine kinase-dependent suppression of a voltage-gated potassium channel. *Mol. Biol. Cell*. 15:4073–4088. <https://doi.org/10.1091/mbc.e03-11-0788>
- Nicklin, P., P. Bergman, B. Zhang, E. Triantafellow, H. Wang, B. Nyfeler, H. Yang, M. Hild, C. Kung, C. Wilson, et al. 2009. Bidirectional transport of amino acids regulates mTOR and autophagy. *Cell*. 136:521–534. <https://doi.org/10.1016/j.cell.2008.11.044>
- Pena, S.D.J., and R.L.M. Coimbra. 2015. Ataxia and myoclonic epilepsy due to a heterozygous new mutation in KCNA2: proposal for a new channelopathy. *Clin. Genet.* 87:e1–e3. <https://doi.org/10.1111/cge.12542>
- Pongs, O., and J.R. Schwarz. 2010. Ancillary subunits associated with voltage-dependent K⁺ channels. *Physiol. Rev.* 90:755–796. <https://doi.org/10.1152/physrev.00020.2009>

- Pongs, O., T. Leicher, M. Berger, J. Roeper, R. Bähring, D. Wray, K.P. Giese, A.J. Silva, and J.F. Storm. 1999. Functional and molecular aspects of voltage-gated K⁺ channel beta subunits. *Ann. N. Y. Acad. Sci.* 868: 344–355. <https://doi.org/10.1111/j.1749-6632.1999.tb11296.x>
- Rasmusson, R.L., M.J. Morales, R.C. Castellino, Y. Zhang, D.L. Campbell, and H.C. Strauss. 1995. C-type inactivation controls recovery in a fast inactivating cardiac K⁺ channel (Kv1.4) expressed in *Xenopus* oocytes. *J. Physiol.* 489:709–721. <https://doi.org/10.1113/jphysiol.1995.sp021085>
- Rettig, J., S.H. Heinemann, F. Wunder, C. Lorra, D.N. Parcej, J.O. Dolly, and O. Pongs. 1994. Inactivation properties of voltage-gated K⁺ channels altered by presence of beta-subunit. *Nature*. 369:289–294. <https://doi.org/10.1038/369289a0>
- Rezazadeh, S., H.T. Kurata, T.W. Claydon, S.J. Kehl, and D. Fedida. 2007. An activation gating switch in Kv1.2 is localized to a threonine residue in the S2-S3 linker. *Biophys. J.* 93:4173–4186. <https://doi.org/10.1529/biophysj.107.116160>
- Rodriguez-Menchaca, A.A., S.K. Adney, Q.-Y. Tang, X.-Y. Meng, A. Rosenhouse-Dantsker, M. Cui, and D.E. Logothetis. 2012. PIP2 controls voltage-sensor movement and pore opening of Kv channels through the S4-S5 linker. *Proc. Natl. Acad. Sci. USA*. 109:E2399–E2408. <https://doi.org/10.1073/pnas.1207901109>
- Ruben, P., and S. Thompson. 1984. Rapid recovery from K current inactivation on membrane hyperpolarization in molluscan neurons. *J. Gen. Physiol.* 84:861–875. <https://doi.org/10.1085/jgp.84.6.861>
- Rudy, B. 1988. Diversity and ubiquity of K channels. *Neuroscience*. 25:729–749. [https://doi.org/10.1016/0306-4522\(88\)90033-4](https://doi.org/10.1016/0306-4522(88)90033-4)
- Rudy, B., J.H. Hoyer, H.A. Lester, and N. Davidson. 1988. At least two mRNA species contribute to the properties of rat brain A-type potassium channels expressed in *Xenopus* oocytes. *Neuron*. 1:649–658. [https://doi.org/10.1016/0896-6273\(88\)90164-X](https://doi.org/10.1016/0896-6273(88)90164-X)
- Sachdev, M., M. Gaínza-Lein, D. Tchapyjnikov, Y.-H. Jiang, T. Loddenkemper, and M.A. Mikati. 2017. Novel clinical manifestations in patients with KCNA2 mutations. *Seizure*. 51:74–76. <https://doi.org/10.1016/j.seizure.2017.07.018>
- Serôdio, P., and B. Rudy. 1998. Differential expression of Kv4 K⁺ channel subunits mediating subthreshold transient K⁺ (A-type) currents in rat brain. *J. Neurophysiol.* 79:1081–1091. <https://doi.org/10.1152/jn.1998.79.2.1081>
- Shi, G., K. Nakahira, S. Hammond, K.J. Rhodes, L.E. Schechter, and J.S. Trimmer. 1996. Beta subunits promote K⁺ channel surface expression through effects early in biosynthesis. *Neuron*. 16:843–852. [https://doi.org/10.1016/S0896-6273\(00\)80104-X](https://doi.org/10.1016/S0896-6273(00)80104-X)
- Shibata, R., K. Nakahira, K. Shibasaki, Y. Wakazono, K. Imoto, and K. Ikenaka. 2000. A-type K⁺ current mediated by the Kv4 channel regulates the generation of action potential in developing cerebellar granule cells. *J. Neurosci.* 20:4145–4155. <https://doi.org/10.1523/JNEUROSCI.20-11-04145.2000>
- Song, W.J. 2002. Genes responsible for native depolarization-activated K⁺ currents in neurons. *Neurosci. Res.* 42:7–14. [https://doi.org/10.1016/S0168-0102\(01\)00305-4](https://doi.org/10.1016/S0168-0102(01)00305-4)
- Steidl, J.V., and A.J. Yool. 1999. Differential sensitivity of voltage-gated potassium channels Kv1.5 and Kv1.2 to acidic pH and molecular identification of pH sensor. *Mol. Pharmacol.* 55:812–820.
- Stirling, L., M.R. Williams, and A.D. Morielli. 2009. Dual roles for RHOA/RHO-kinase in the regulated trafficking of a voltage-sensitive potassium channel. *Mol. Biol. Cell*. 20:2991–3002. <https://doi.org/10.1091/mbc.e08-10-1074>
- Syrbe, S., U.B.S. Hedrich, E. Riesch, T. Djémié, S. Müller, R.S. Møller, B. Maher, L. Hernandez-Hernandez, M. Synofzik, H.S. Caglayan, et al. EuroEPINOMICS RES consortium. 2015. De novo loss- or gain-of-function mutations in KCNA2 cause epileptic encephalopathy. *Nat. Genet.* 47:393–399. <https://doi.org/10.1038/ng.3239>
- Tsaur, M.L., C.C. Chou, Y.H. Shih, and H.L. Wang. 1997. Cloning, expression and CNS distribution of Kv4.3, an A-type K⁺ channel alpha subunit. *FEBS Lett.* 400:215–220. [https://doi.org/10.1016/S0014-5793\(96\)01388-9](https://doi.org/10.1016/S0014-5793(96)01388-9)
- Williams, M.R., J.C. Markey, M.A. Doczi, and A.D. Morielli. 2007. An essential role for cortactin in the modulation of the potassium channel Kv1.2. *Proc. Natl. Acad. Sci. USA*. 104:17412–17417. <https://doi.org/10.1073/pnas.0703865104>
- Xu, J., W. Yu, J.M. Wright, R.W. Raab, and M. Li. 1998. Distinct functional stoichiometry of potassium channel beta subunits. *Proc. Natl. Acad. Sci. USA*. 95:1846–1851. <https://doi.org/10.1073/pnas.95.4.1846>
- Yan, R., X. Zhao, J. Lei, and Q. Zhou. 2019. Structure of the human LAT1-4F2hc heteromeric amino acid transporter complex. *Nature*. 568: 127–130. <https://doi.org/10.1038/s41586-019-1011-z>
- Yang, E.-K., K. Takimoto, Y. Hayashi, W.C. de Groat, and N. Yoshimura. 2004. Altered expression of potassium channel subunit mRNA and alpha-dendrotoxin sensitivity of potassium currents in rat dorsal root ganglion neurons after axotomy. *Neuroscience*. 123:867–874. <https://doi.org/10.1016/j.neuroscience.2003.11.014>

Supplemental material

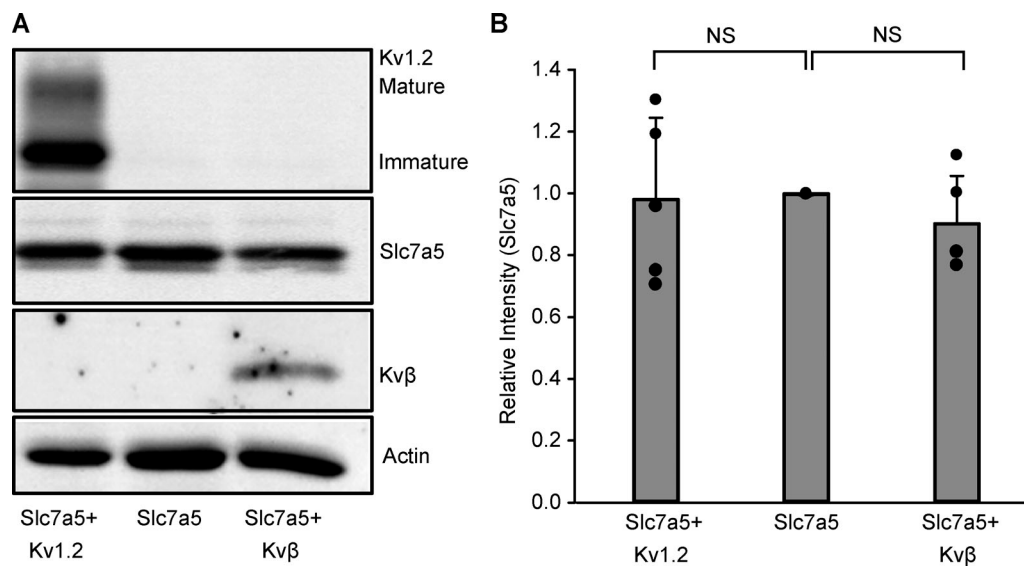


Figure S1. **Kv1.2 and Kvβ do not influence Slc7a5 expression.** (A) Representative Western blot of overexpressed mCherry-tagged Slc7a5 protein ± Kv1.2 and ± Kvβ from HEK293 cells transfected as in Fig. 1A for 72 h. Actin was used as a loading control. (B) Densitometry measurements of mCherry-tagged Slc7a5 protein bands. Data from individual experiments are superimposed on bars that depict the mean values ± SD ($n = 4-5$ independent Western blot experiments). ANOVA followed by Dunnett's post hoc test was used to compare between groups. No statistical difference was observed between any groups.

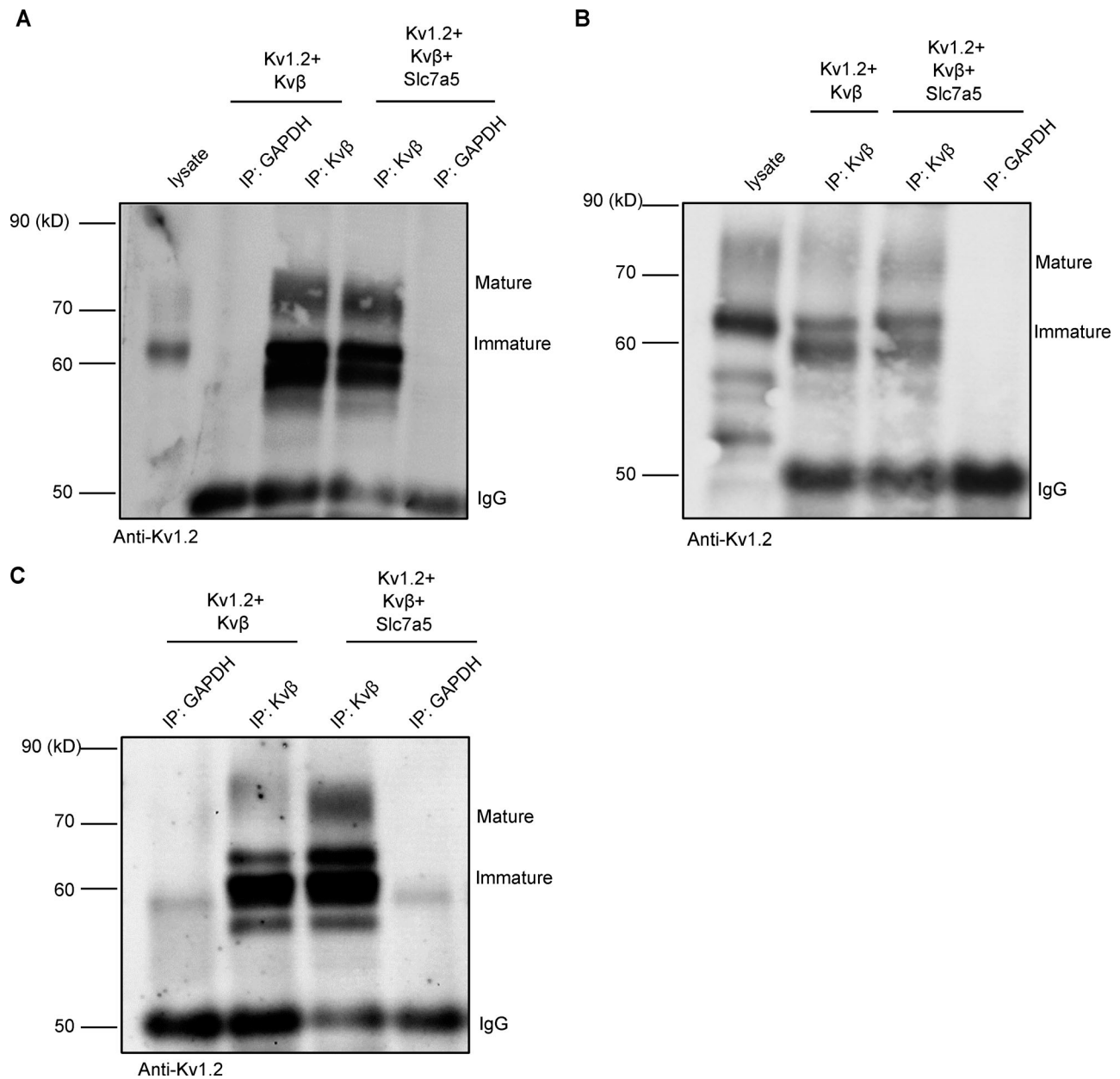


Figure S2. **Slc7a5 does not interfere with co-IP of Kvβ and Kv1.2.** Combinations (as indicated in Fig. 1 A) of Kv1.2, Slc7a5, Kvβ, and GFP were expressed in HEK293 cells. (A–C) Co-IP from three independent experiments showing that the interaction between Kv1.2 and Kvβ is enhanced in the presence of Slc7a5. GAPDH was used as a negative control. IgG is used as the loading control.

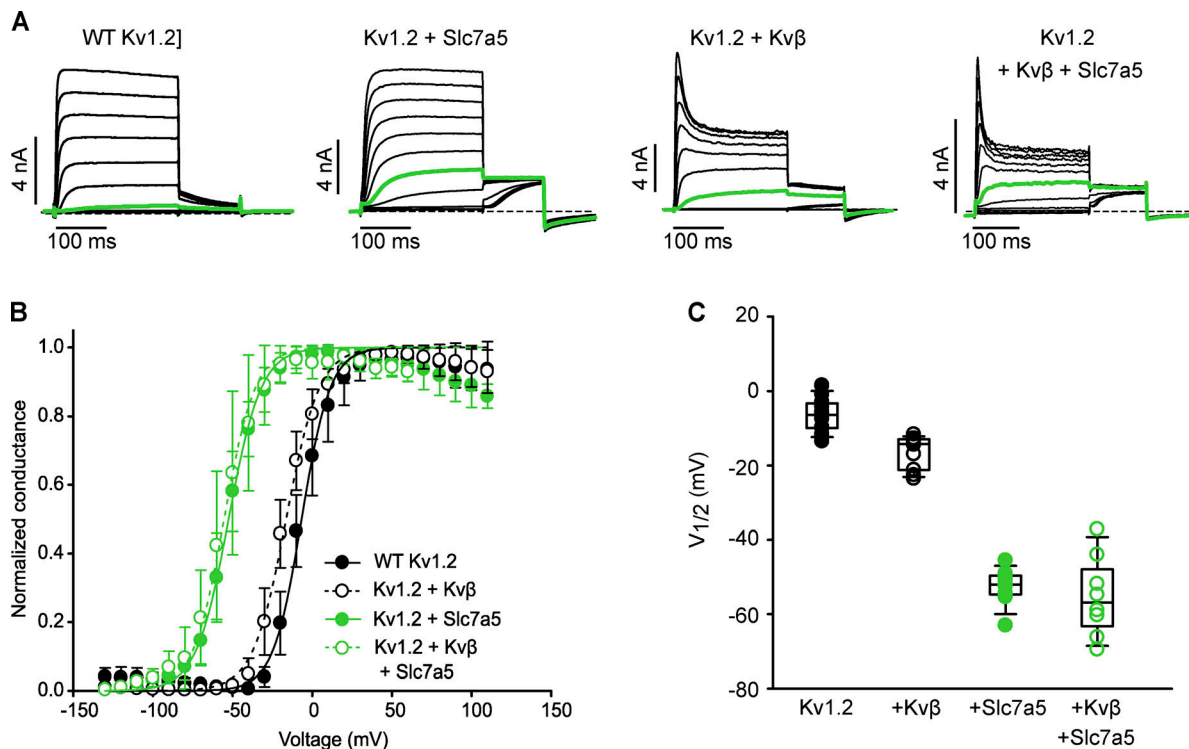


Figure S3. Slc7a5 and Kvβ influence gating properties for WT Kv1.2. (A) Combinations of WT Kv1.2, Slc7a5, and Kvβ were transfected in LM mouse fibroblasts. Cells were hyperpolarized to -120 mV for 30 s before recording to disinhibit Kv1.2 currents. A 100-ms depolarization potentiating prepulse to $+60$ mV was delivered to relieve Kv1.2 use-dependent activation at the beginning of each sweep. G-V relationships were measured by stepping between -130 and 110 mV (150 ms in 10-mV steps, -100 -mV holding potential), followed by a tail current voltage of -30 mV. Representative current traces of the activation curves are shown, with the pulse to -20 mV highlighted in green. (B) G-V plots were generated by analyzing the tail current amplitudes at -30 mV and fitting with a Boltzmann function (WT Kv1.2 $V_{1/2} = -6.7 \pm 5$ [mean \pm SD], $k = 10 \pm 3$, $n = 11$ individual cells recorded; Kv1.2 + Kvβ $V_{1/2} = -16.4 \pm 4.5$, $k = 10.3 \pm 1.8$, $n = 10$; Kv1.2 + Slc7a5 $V_{1/2} = -52.5 \pm 4.9$, $k = 9.50$, $n = 9$; Kv1.2 + Kvβ + Slc7a5 $V_{1/2} = -55 \pm 11$, $k = 10.0 \pm 1.5$, $n = 8$). (C) $V_{1/2}$ of individual cells from each group in A. Box plots depict the median, 25th, and 75th percentiles (box) and the 10th and 90th percentiles (whiskers).

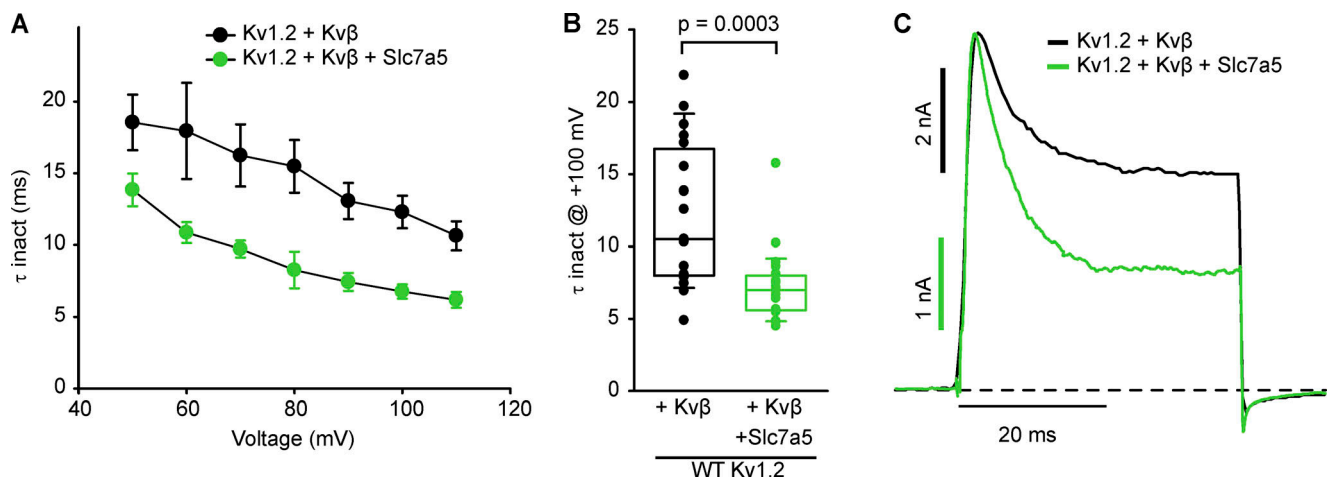


Figure S4. Coexpression of Slc7a5 accelerates Kvβ-mediated inactivation kinetics in WT Kv1.2 channels. (A) LM cells were transfected with WT Kv1.2 + Kvβ or WT Kv1.2 + Kvβ + Slc7a5 with transfection ratios as previously mentioned. Cells were hyperpolarized to -120 mV for 30 s before recording, to disinhibit Kv1.2 currents. Time constants of inactivation (τ_{inact}) were calculated from a single exponential fit of the inactivating current at depolarizing sweeps from 50 to 110 mV in 10-mV increments for 100 ms from a -100 -mV holding potential ($n = 19$ –23 individual cells recorded for each group). (B) τ_{inact} of individual cells from each group in A were obtained from the inactivating currents at $+100$ mV from a -100 -mV holding voltage ($n = 19$ –23 individual cells recorded for each group; Student's t test was used to compare the Slc7a5 treatment group versus the respective control; P values are denoted above the box plots). (C) Representative traces of LM cells were depolarized to $+100$ mV for 40 ms from a -100 -mV holding potential. Box plots depict the median, 25th, and 75th percentiles (box) and the 10th and 90th percentiles (whiskers).

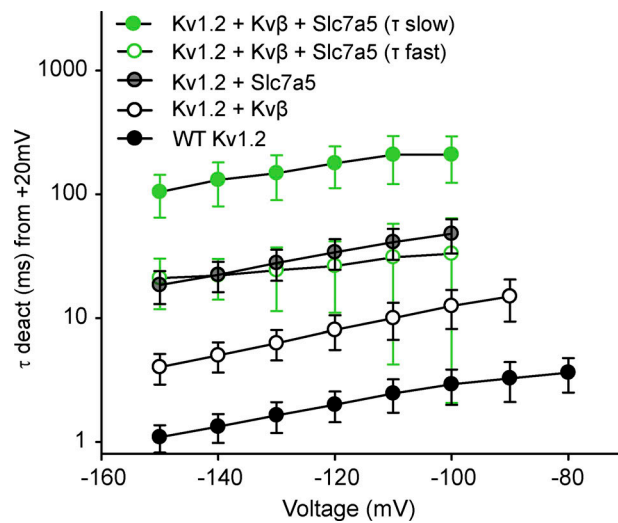


Figure S5. **Functional interactions of Slc7a5 and Kvβ influence the deactivation kinetics of Kv1.2.** LM cells were transfected with combinations of WT Kv1.2, Kvβ, and Slc7a5 as previously mentioned. Cells were depolarized to +20 mV for 200 ms followed by repolarizing steps from −60 to −150 mV in 10-mV increments for 600 ms before returning to a −100-mV holding potential. Time constants of deactivation (mean ± SD) were calculated from single (WT Kv1.2; Kv1.2 + Kvβ; Kv1.2 + Slc7a5) or double (Kv1.2 + Kvβ + Slc7a5) exponential functions of the deactivation tail currents obtained from repolarizing voltage sweeps of −60 to −150 mV from a +20-mV depolarizing step ($n = 11$ –18 individual cells recorded for each group).

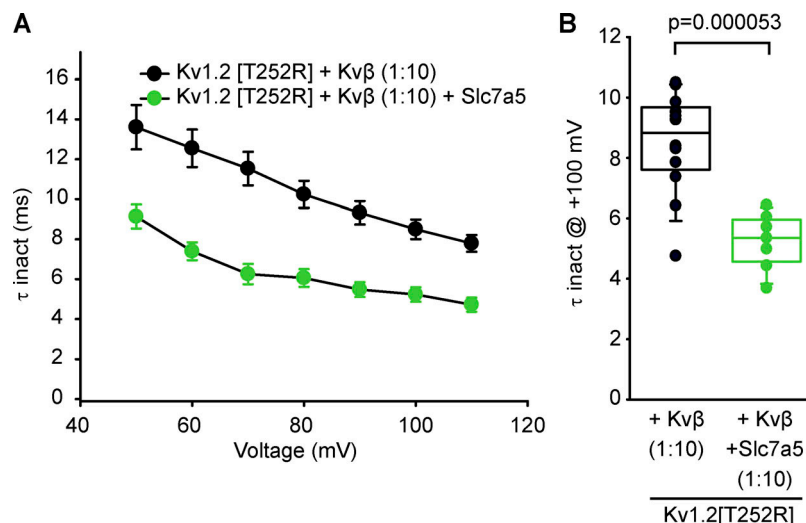


Figure S6. **A high Kvβ:Kv1.2 transfection ratio does not cause accelerated inactivation and does not prevent functional effects of Slc7a5.** (A) LM cells were transfected with Kv1.2(T252R) and Kvβ in the absence or presence of mCherry Slc7a5. Transfection ratios were (with Kv1.2 maintained constant using GFP) Kv1.2:Kvβ, 1:10; Kv1.2:Kvβ:Slc7a5, 1:10:0.5. Cells were hyperpolarized to −120 mV for 30 s before recording to disinhibit Kv1.2 currents. Time constants of inactivation (τ_{inact}) were calculated from a single exponential fit of the inactivating current at depolarizing sweeps from 50 to 110 mV in 10-mV increments for 100 ms from a −100-mV holding potential (mean ± SEM; $n = 7$ –12 individual cells recorded for each group). (B) τ_{inact} of individual cells from each group in A were obtained from the inactivating currents at +100 mV from a −100-mV holding voltage ($n = 7$ –12 individual cells recorded for each group). Student's t test was used to compare the Slc7a5 treatment group versus the respective control; P values are denoted above the box plots. Box plots depict the median, 25th, and 75th percentiles (box) and the 10th and 90th percentiles (whiskers).